12-2021

Incorporation of Zinc in pre-Alloyed CuIn[Zn]S2/ZnS Quantum Dots

Jean Carlos Morales Orocu
University of Arkansas, Fayetteville

Incorporation of Zinc in pre-Alloyed $CuIn[Zn]S_2/ZnS$ Quantum Dots

A thesis submitted in partial fulfillment
of the requirements for the degree of
Master of Science in Microelectronics-Photonics

by

Jean C. Morales Orocu
University of Arkansas
Bachelor of Science in Chemical Engineering, 2018

December 2021
University of Arkansas

This thesis is approved for recommendation to the Graduate Council.

Colin D. Heyes, Ph.D.
Thesis Director

Jingyi Chen, Ph.D
Committee Member

Fisher Yu, Ph.D.
Committee Member

Robert H. Coridan, Ph.D.
Committee Member

Matt Leftwich, Ph.D.
Ex-Officio Member

The following signatories attest that all software used in this thesis was legally licensed for use by Jean C. Morales Orocu for research purposes and publication.

Mr. Jean C. Morales Orocu, Student	Dr. Colin D. Heyes, Thesis Director

This thesis was submitted to http://www.turnitin.com for plagiarism review by the TurnItIn company's software. The signatories have examined the report on this thesis that was returned by TurnItIn and attest that, in their opinion, the items highlighted by the software are incidental to common usage and are not plagiarized material.

Dr, Matthew Leftwich, Program Director	Dr. Colin D. Heyes, Thesis Director

Abstract

Since the early 2000s heavy-metal-free quantum dots (QDs) such as $CuInS_2$/ZnS have attempted to replace CdSe, their heavy-metal-containing counterparts. $CuInS_2$/ZnS is synthesized in a two-step process that involves the fabrication of $CuInS_2$ (CIS) nanocrystals (NCs) followed by the addition of zinc precursors. Instead of the usual core/shell architecture often exhibited by binary QDs, coating CIS QDs results in alloyed and/or partially alloyed cation-exchange (CATEX) QDs. The effect that zinc has on the properties of CIS NCs was studied by incorporating zinc during the first step of the synthesis.

Different In:Cu:Zn ratios were employed in this study, maintaining a constant 4:1 In:Cu molar ratio. When a 4:1:4 In:Cu:Zn molar ratio was employed, the photoluminescence quantum yield (PL QY) increased from 12% (for the Zn-free CIS QDs) to 28%, and the fluorescence lifetime increased from 191 ns to 293 ns. The polydispersity of these NCs was also reduced, shrinking the full-width-at-half-maximum (FWHM) by 40 nm, while only increasing the average particle diameter from 3.3 nm to 3.9 nm.

The superior optical performance of Zn-containing QD cores was, nevertheless, not observed after NCs underwent 24 hours of cation exchange. Zn-free QD cores reached PL QY of up to 75% upon cation exchange, while Zn-containing cores showed PL QY as low as 35%. After six hours of reaction zinc overtook indium and copper, making up above 97% of the metallic elements present in all CATEX QDs. The presence of zinc prior cation exchange did not influence the fluorescence lifetime, with 300 ns being measured for nearly all CATEX QDs, but had a detrimental effect on particle growth. Quantum Dot cores that lacked zinc showed an average particle size of over seven nanometers, a significant increase when compared to the minimal growth of over four nanometers experienced by those with highest zinc content.

Acknowledgements

When I started grad school, I was afraid of the words "writing a thesis" but with sacrifice, perseverance, and the support of so many people I was no longer afraid. I want to use this space to express gratitude to some of those individuals.

Firstly, I want to start by thanking my family. To my parents Celia and Alirio who have always encouraged me to achieve my goals and be the best version of myself. My sister Celiris for being the most loving sibling and my aunt Edisa for always having me in her prayers. Despite being 3,000 miles away I could not have done this without all of you.

Secondly, I want to thank my major professor Dr. Colin Heyes and my former academic advisor Dr. Rick Wise for the immense guidance provided throughout my graduate career; and to the members of my committee Dr. Robert Coridan, Dr. Jingyi Chen, and Dr. Fisher Yu for sharing their wisdom and knowledge with me.

I also want to express gratitude to Erik Pollock and Barry Shaulis from the Trace Element and Radiogenic Isotope Lab at the University of Arkansas; to Dr. Benamara and Dongdong Yu from the Nano & Biomaterials Characterization Facility at the University of Arkansas; to James from Dr. Coridan's Lab and Isabelle from Dr. Chen's Lab; to Renee and Dr. Leftwich, who kept me on track; and my lab mates: Anh, Mamello, Colette, and Dustin who shared their knowledge and experience with me.

Lastly, I want to thank my friends. Alexis, Arantxa, and John for their unconditional support, and my dog Luke, an incredible source of comfort during this journey, as well as other friends and people that I did not have space to mention on this page, thank you!

This program is financially supported by the National Science Foundation under Grant No. CHE-1255440 Any opinions, findings, and conclusions or recommendations expressed in

this material are those of the author and do not necessarily reflect the views of the National Science Foundation.

Dedication

This thesis is dedicated to my late grandmother Juana who passed away in October of 2020. This work is also dedicated to the thousands that lost their life in the midst of the COVID-19 pandemic.

Table of Contents

List of Figures

Chapter 1: Literature Review & Background

1.1. Quantum Dots

During the past two decades, the field of nanotechnology has experienced a boom in research, particularly on investigation related to semiconductor nanocrystals (NCs) also known as quantum dots (QDs), first studied in the early 90's [1]. Quantum dots are artificial semiconductor nanoparticles with sizes approximately ranging between two and ten nanometers containing from 100 to 10,000 atoms. These nanocrystals exhibit unique optical and electronic properties that differ from those showed by materials of similar elemental composition at larger particle sizes.

The divergence in properties between QDs and bulk materials is caused by a phenomenon known as quantum confinement. This is observed when the particle diameter of a semiconductor material reaches such small dimensions that it can be compared to the de Broglie wavelength of the electron wavefunction, going beyond the Bohr exciton radius of such material. For instance, after a bulk-size semiconductor material has been exposed to a source of light, two activated charges are created, a negatively charged electron and a positively charged hole. These charges can move freely in the bulk material causing a continuous charge flow across the material.

In contrast, when a particle size reaches dimensions on the nanoscale, the electron and hole charges are forced to be together or confined; therefore, leading to an increase in the amount of energy necessary to separate both charges. This energy is known as the energy bandgap and increases as particle size gets smaller and the Bohr exciton radius, an intrinsic property of materials, is approached. For this reason, QDs are often referred to as artificial atoms [1].

1.1.1. Architecture

1.1.1.1. Core

The QD core, in an ample sense, refers to the electron-hole recombination centers in NCs. Without proper coating with a second material, QD cores are poorly passivated due to presence of surface defects and lack of enough crystalline character. Poor passivation results in low-performing optical and electronic properties such as low PL QY, lower fluorescence lifetimes, and constraints in tunability. Quantum dot cores are also often found to have higher levels of toxicity, especially for heavy-metal-containing NCs [2]–[4]. Quantum dot cores, alone, are highly prone to be degraded by external factors in the environment that could not only hurt their performance, but also result in the release of QD contents to the environment. This could cause serious repercussions since toxic contents present in the QD core are known to trigger cell death [2].

1.1.1.2. Shell

Quantum dots are versatile nanoparticles whose properties can be easily manipulated by changing their size and/or composition by coating them with other materials. This coating often referred to as “shell” optimizes the optical and electronic properties of nanoparticles by eliminating or inhibiting the effect of trap states and surface defects generally present in QDs [5]. This coating has been found to have remarkable effect on reducing QD cytotoxicity [6]. Shells also serve as a protective coating layer that increments stability and the life span of NCs [7]. Quantum dot shelling is an effective way to control size in QDs while simultaneously improving their performance.

1.1.1.3. Alloyed QDs

Unlike most binary QDs, some ternary QDs such as $CuInS_2$ exhibit a different coating mechanism. Upon being coated with a second material, $CuInS_2$ QDs do not show a core-shell architecture as shown in Figure 1-a, instead, their structural composition can be better described as that of a partial alloy (Figure 1-c) [8]–[10] . In other words, although coating materials are most likely found near the surface of $CuInS_2$-ZnS nanoparticles, there may still be some level diffusion of coating materials into the QD core and/or displacing some of the QD core contents towards the outer atom layers of the nanocrystals. Figure 1 a-c shows a visual representation of a pure core/shell QDs, one that has undergone cation exchange, and a partially alloyed QD, respectively.

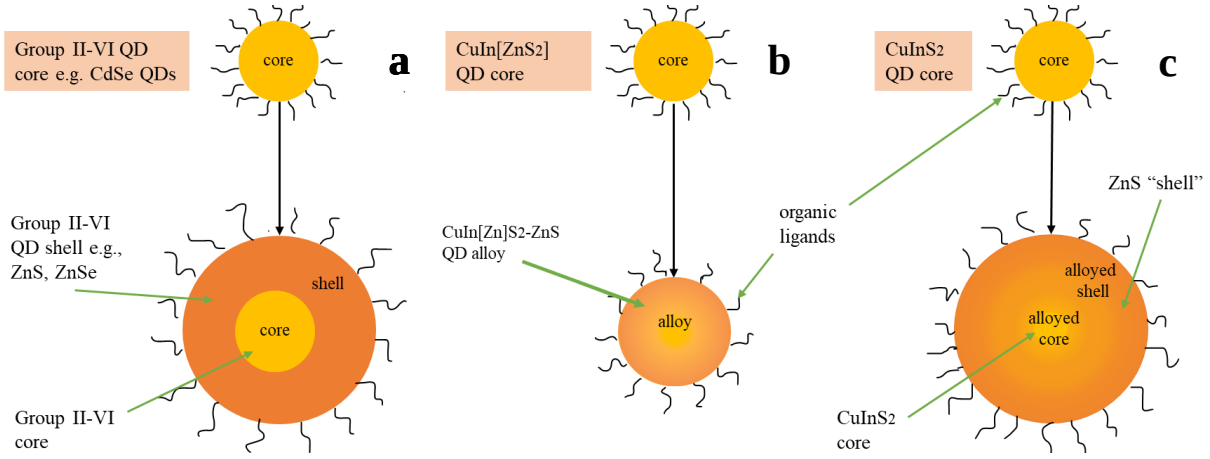

Figure 1 – Diagram depicts the traditional shelling of a nanocrystal (a), a cation exchange alloy (b) and an alloyed combination of both mechanisms (c)

Cation exchange can also lead to recombination centers be found closer to the NC surface, or even the creation of multiple recombination centers unevenly distributed throughout the nanoparticle lattice.

1.1.2. Optical and Electronic properties

The optical and electronic properties of QDs strongly depend on their size, therefore a monodisperse nanocrystal population is preferred over one that is polydisperse. In general, Ostwald ripening governs the growth of nanoparticles in a reaction mixture [11]. The theory behind Ostwald ripening demonstrates that large particles grow while small particles dissolve, resulting in a broad size distribution. Studies show that size focusing can occur at a high oversaturation condition, circumventing Ostwald ripening [11]. Ostwald ripening can also result in size-focusing when a broad starting size distribution is kept reacting.

1.1.2.2. Photoluminescence quantum yield (PL QY)

The most remarkable property that QDs exhibit is photoluminescence (PL), the emission of photons as electrons excited through photoexcitation to a higher energy level relax back to their ground state. Photoluminescence can take place as two independent phenomena, fluorescence, and phosphorescence. Fluorescence can be defined as a radiative process in which an excited fluorophore decays to ground state through the emission of photons with a time delay in the order of nanoseconds. The vast majority of photoluminescence that QDs exhibit occurs as fluorescent events, and a small portion as phosphorescence [12].

Once electrons have been excited to a higher electronic energy level, electrons go through a non-radiative process known as vibrational relaxation where they go down to the least energetic vibrational level of the first excited electronic energy level. Fluorescence can only occur once electrons are in the lowest vibrational level of the excited electronic state. Electrons can also relax through internal conversion, a non-radiative process that is detrimental for a quantum dot PL QY. Phosphorescence occurs when intersystem crossing takes place from a

singlet to a triplet state causing a forbidden (same spin) transition. In QDs, radiative and non-radiative relaxation pathways are closely associated with the presence or absence of trap states. Figure 2 illustrates the role of trap state passivation in the radiative outcomes of electron relaxation in QDs.

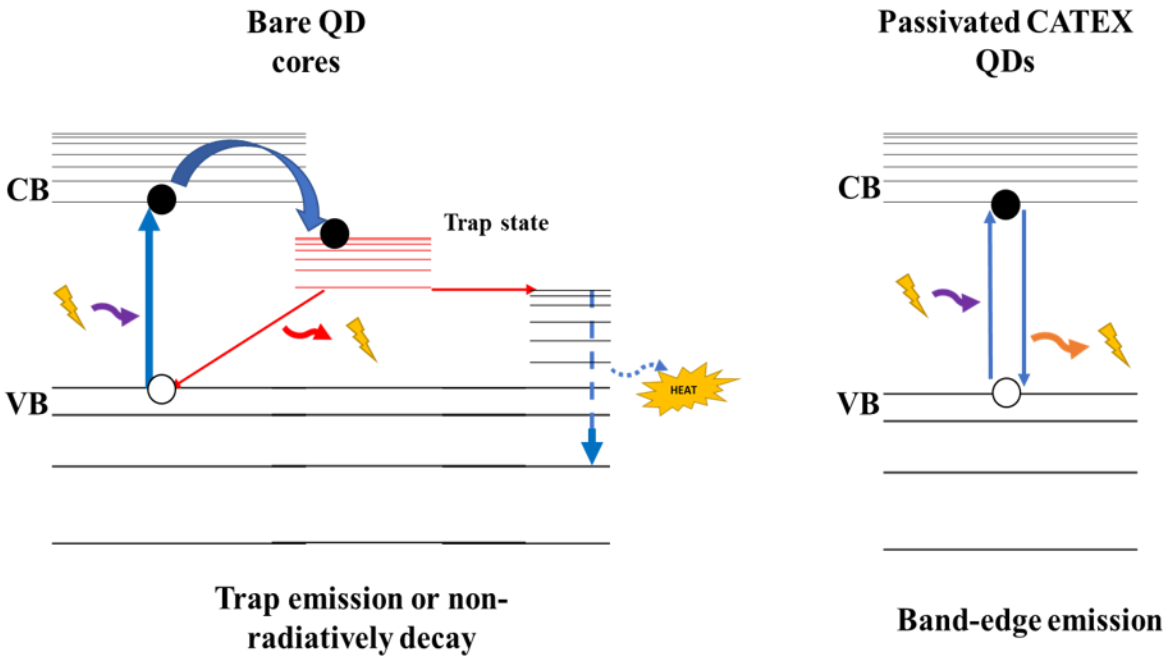

Figure 2 – Effect of QD passivation on trap states radiative decay

When NCs absorb light, the number of emitted photons is usually lower than the number of absorbed photons. This fluorophore emission efficiency is known as quantum yield, defined as the ratio of emitted photons divided by the ratio of absorbed photons as displayed in Equation 1 where k_f, k_{nr}, k_t represent the fluorescence, non-radiative, and energy transfer rate constants during electron relaxation events [13].

$$QY = \frac{\#\ \text{photons emitted}}{\#\ \text{photons absorbed}} = \frac{k_f}{k_f + k_{nr} + k_t} \qquad \text{Equation 1}$$

1.1.2.3. Fluorescence Lifetime

The average time at which molecules remain in the excited electronic state between the initial excitation and the subsequent photon emission is referred to as fluorescence lifetime. If a homogenous population is being analyzed, the fluorescence decay that results from the photon emission is a single-exponential function [13]. Mathematically, the fluorescent lifetime is the time constant of this function and can be calculated as the reciprocal sum of the rate constant of all possible paths of return from an electronic excited state to an electronic ground state.

The exponential decay function of QDs has been extensively studied in previous literature and their decay appears to follow a multiexponential behavior, though the number of exponential terms that should be included is a common point of disagreement [14]–[16].

$$k_r = \frac{QY}{\tau_{fl}} \qquad \text{Equation 2}$$

$$k_{nr} = k_r - \frac{1}{\tau_{fl}} \qquad \text{Equation 3}$$

1.1.2.4. Fluorescence Intermittency or blinking

The phenomenon of fluorescence intermittency, most commonly known as blinking, remains one of the unsolved problems of quantum mechanics due to competition between the radiative and nonradiative rate constants during a fluorophore relaxation event. There are multiple models that have attempted to provide an explanation to this phenomenon [17]–[20] including various works at Heyes Group [21]–[23], but none has yet accounted for all variables. Blinking experiments are beyond the scope of this work but will be a topic of future research.

1.1.2.5. Bandgap

The bandgap energy is by definition the difference in energy between the valance and conduction bands in a semiconductor material. The energy bandgap is, therefore, directly linked to other properties of semiconductor materials such as the emission wavelength (color of the NCs) and the quantum confinement (nanoparticle size).

Due to quantum confinement effects, smaller particles require more energy to allow electrons to overcome the energy bandgap so they can move freely in the conduction band. This higher energy input results in high-frequency/low-wavelength photonic emissions. Quantum confinement effects cause small NCs to emit high-energy blue light, and larger NCs to emit low-energy red light. Quantum dots are great semiconductors due to the simplicity with which one can control their size, and therefore, tune their energy bandgap and emission spectra.

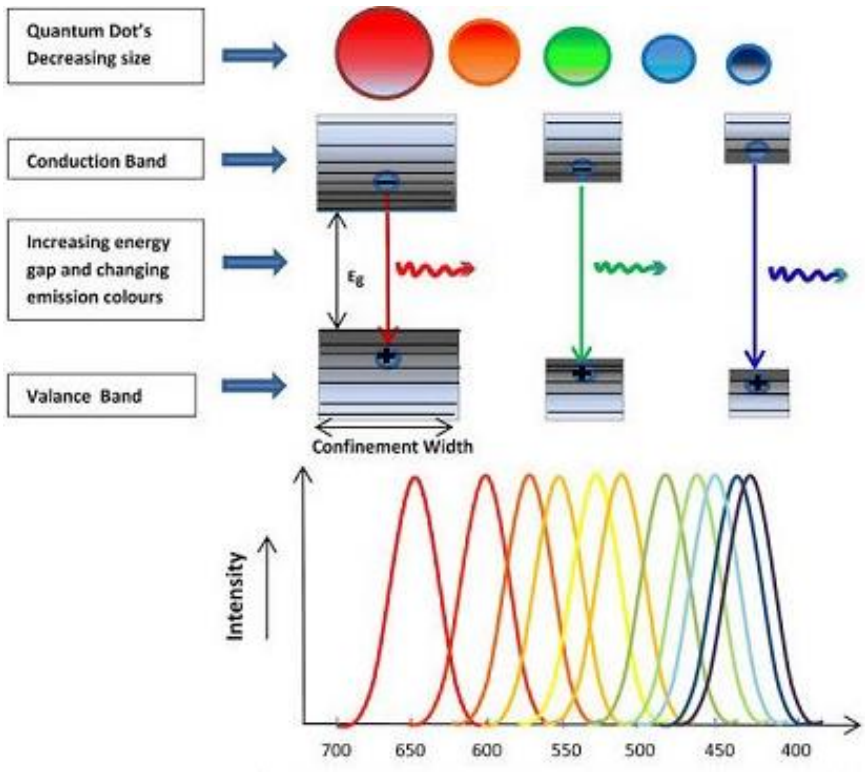

Figure 3 - Relation between energy band gap, emission spectra and QD particle size

1.1.3. Binary Quantum Dots

Quantum dots have become a prominent field of study in nanotechnology over the last few decades due to the versatility of their properties and the relative ease with which they can be tuned to fulfill specific requirement for several applications. Quantum dots can be used across many fields in nanoscience, engineering, and biotechnology that include applications related to biological imaging [24]–[26], photovoltaic devices [27]–[29] photodetectors [30]–[32], photocatalysts [33]–[35] , and LEDs [36]–[38]. A much higher photostability, narrower emission spectra and broad excitation bands have led to QDs becoming a great competitor to organic dyes and fluorescent proteins for certain applications in medicine [39].

1.1.3.2. Cadmium Selenide QDs

The most prominent examples of colloidal quantum dots in industry are binary quantum dots where a chalcogen interacts with a metal cation, usually lead, indium or cadmium. Cadmium selenide QDs have become a standard in the colloidal quantum dot industry since their introduction.

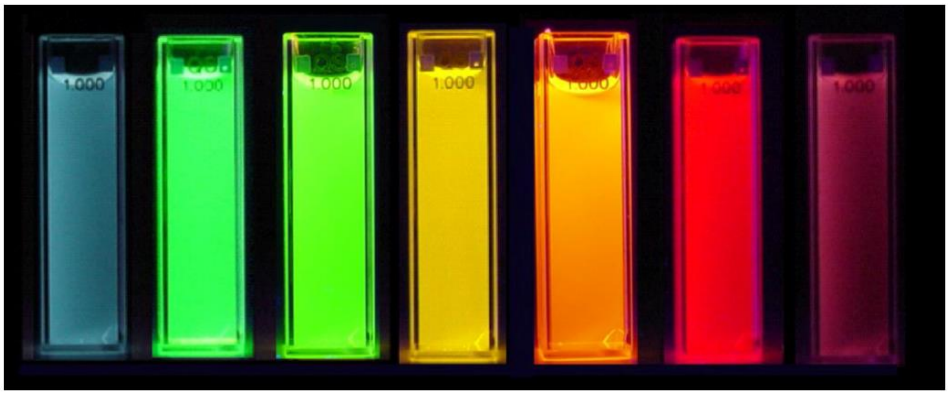

Figure 4 - CdSe QDs with sizes ranging from 2.5 nm (blue) to 6.5 nm (red) excited with the same 366 nm UV lamp

Cadmium selenide QDs have relatively short fluorescent lifetimes (about 20-50 ns), are monodisperse, and upon shelling, exhibit PL QYs close to unity [40]. The vast majority of the work done on studying QDs has been done on binary II-VI, IV-VI, III-V QDs mainly CdE, PbE (E = Se, Te, S) [41], [42] and InP [43] respectively. Their toxicity is heavily mitigated by shelling the QD core with a second material several times isolating the QD core contents from the surrounding environment.

1.1.3.3. Environmental concerns

Concerns regarding the toxicity of heavy-metal-containing binary QDs have been an ongoing topic for years due to the presence of cadmium and lead, transition heavy metals, known to trigger cell death [2] representing a serious hazard for applications in medicine and biology. For applications outside the biological and medical field, such as light-emitting diodes and photovoltaic cells [27], it is acceptable to neglect some of the concerns regarding toxicity present in binary heavy-metal-containing quantum dots; nonetheless, long term degradation still represent a hazard for the environment [4]. Disposal and accumulation of these materials need to be addressed as serious environmental issues.

Applications such as bioimaging, bio-tracking, and photodetection demand that quantum dots be compatible with biological systems, reason why CdSe QDs lack approval from the international community for those purposes. There has been a significant number of efforts that have attempted to reduce the cytotoxicity inherent to CdSe QDs, and some have been successful to an extent.

Cytotoxicity of CdSe quantum dots has been found to decrease considerably upon shelling with multiple ZnS layers [44]. In addition, shelling with a second material, like ZnS,

serves as an agent that reduces trap states in quantum dots, greatly enhancing radiative properties of nanoparticles. Regardless of the mitigated toxicity of shelled CdSe QDs, there still exists reservations regarding the use of shelled CdSe quantum dots in the medical field due to degradation issues at the single quantum dot level that could eventually liberate traces of cadmium, representing a serious hazard for the patient.

1.1.4. Ternary Quantum Dots

1.1.4.2. $CuInS_2$/ZnS Quantum Dots

Most of the information available in current literature regarding photoluminescence properties of QDs is limited, and most of which has solely been performed on cadmium containing binary QDs, and almost non-existent for ternary and quaternary NCs. Additionally, even though CIS-ZnS QDs have been proposed as an alternative to heavy-metal-containing QDs, recent studies have found that CIS NCs do show some level of toxicity when not shelled [45].

The ternary and quaternary nature of these particles increases the complexity of relating structure and composition to optical and electronic properties. CIS-ZnS QDs have been found to achieve a quantum yield of 65% [23] , making fluorescence one of their most valuable properties. As a matter of fact, their fluorescence lifetimes are ten to 50 times longer than binary QDs, opening doors to additional applications based on fluorescence lifetime such as fluorescence lifetime imaging (FLIM).

Having reliable knowledge on the relationship between structure, composition, and fluorescence properties, such as blinking, is vital to realize the full potential that CIS-ZnS QDs possess. For instance, understanding how varying amounts of initial reagents in CIS-ZnS QDs

affects blinking is imperative to formulate pathways through which fluorescence intermittency may occur. These pathways need to be known so that blinking can be controlled for it to be mitigated or enhanced depending on parameters that the NCs need to suffice for specific applications.

Due to the ternary nature of CIS QDs, the number of imperfections contained in their lattice is higher than those found in binary II-VI QDs. Interestingly enough, these surface defects act as trap states and fluctuations that can effectively localize electrons and holes, resulting in abnormally long fluorescent lifetimes [46]. The fact that $CuInS_2$-ZnS QDs do not contain heavily toxic elements makes them excellent candidates to replace cadmium-containing binary QDs, especially in biological applications.

1.2. Characterization:

1.2.1. Optical

The determination of the PL QY of a sample is the first step in the characterization process of a fluorescent nanoparticle. To calculate the PL QY of a sample it is necessary to measure the number of photons that the sample absorbs upon being struck with light, and the number of photons the samples emits upon relaxation to ground state. UV-vis absorption spectroscopy and fluorescence emission spectroscopy allow us to determine the amount of light that a sample absorbs and emits respectively.

A fairly common procedure to determine the fluorescence quantum yield of a sample is by comparing it to a dye of known PL QY as shown in Equation 4. This comparison, also known as relative quantum yield, is only applicable when the absorbance of both the dye and the quantum dot sample are measured at the excitation wavelength and their emission spectra need to display

an overlap. Rhodamine 6G, with a quantum yield of 95%, is one of the most widely used dyes to perform this comparative analysis [47].

$$QY_{smp} = QY_{ref} \frac{a_{ref}}{a_{smp}} \frac{A_{smp}}{A_{ref}} \left(\frac{n_{smp}}{n_{ref}}\right)^2 \quad \text{Equation 4}$$

where “a” stands for the absorbance, “A” the area under the curve of the emission spectrum, and “n” the diffraction coefficient of the solvent used. The subscripts “ref” and “smp” are the reference (R6G dye) and sample (QDs)

1.2.2. Structural

Because the compound light microscope has a resolution near the wavelengths of light, it is necessary to utilize a tool that would resolve particles in the nanoscale. From both SEM and TEM microscopes, TEM has a much better resolution because several projector lenses magnify the image after it has passed through the sample. Therefore, the resolution of TEM is usually better than that of SEM by a factor of ten or perhaps more depending on each individual instrument. Quantum dots dimensional characteristics such as size and shape can be observed and measured by means of TEM microscopy.

Transmission electron microscopy (TEM) is suitable for the analysis of individual and aggregates of nanoparticles. The transmission electron microscope projects an image by focusing a high-energy electron beam onto a properly prepared sample. Then, the electron beam goes through the sample, and subsequently through several lenses until it finally projects an image on a fluorescent plate.

When it is necessary to study particles beyond the TEM resolution limit. High-resolution transmission electron microscopy (HR-TEM) is a good option and can usually resolve down to

the atomic regime. Although a low resolution TEM suffices when performing size distribution analyses, high-resolution transmission electron microscopes are necessary to be able to assign lattice parameters to single quantum dots [48].

1.2.3. Elemental

Inductively coupled plasma mass spectrometry (ICP-MS) is a vital tool that allows the analyst to determine elemental compositions of an ionic sample. ICP-MS employs inductively coupled plasma to atomize the sample creating detectable monoatomic ions [49].

X-ray photoelectron spectroscopy (XPS) is necessary to analyze the surface chemistry of nanoparticles [50]. A collision between an X-ray photon and the surface of an object results in the ejection of a core electron when the X-ray photon has sufficient energy. X-ray photoelectron spectroscopy measures the energy difference between the ejected electron and the binding energy of that electron. In fact, this energy difference is an intrinsic property of each specimen, thus, allowing analysts to identify chemical species being studied. In an experiment, a monochromatic beam of X-ray photons is shot to the surface of the analyte, and an energy analyzer measures the energy difference, which is then detected, decoded, and displayed as a spectrum.

1.3. Aim of this study

1.3.1. CuIn[Zn]S_2/ZnS QDs

This investigation is primarily concerned with the utility of $CuInS_2$-ZnS QDs in applications within the field of single-molecule spectroscopy. Furthermore, the fact that $CuInS_2$-ZnS QDs have lifetimes ten to fifty times longer than some of their binary counterparts has

promising applications based on fluorescence lifetime such as fluorescence-lifetime imaging microscopy (FLIM).

It has been found that adding a ZnS shell to $CuInS_2$ cores causes a blueshift in the CIS emission spectrum, rather than the redshift that is observed in cadmium based QDs. This is due to a certain degree of ion exchange between copper, indium and/or zinc occurring at the QD core.

This study involves the characterization of the structure and composition of these nanocrystals using, XPS, HR-TEM and ICP-MS methods. Finally, this will be compared to fluorescence quantum yield, fluorescence lifetime data to make correlations between the composition/architecture of the nanocrystals and the optical properties to determine the possible mechanisms underlying the optical and electronic properties of these materials.

The effects that incorporating zinc into the CIS QD core prior to shelling have on the electronic and optical properties of CIS-ZnS cation-exchange QDs are the main focus of this work.

Chapter 2: Materials and Methods

2.1. Reagents

Copper iodide (CuI) 99.999%, and 1-dodecanethiol (DDT) 98% were purchased from Sigma Aldrich; zinc stearate, ($Zn(st)_2$) and 1-octadecene (ODE) 90% were purchased from Acros; indium acetate ($In(Ac)_3$) 99.99% was purchased from Alpha Aesar. Methanol, hexane, and acetone were purchased from VWR International.

2.2. Synthesis

2.2.1. Synthesis of the core

Four types of QD cores were synthesized. The first type consisted in Zn-free CIS QDs which followed a procedure developed in previous literature. For this, 0.25 mmol of CuI, (0.048g) and 1.0 mmol of $In(Ac)_3$ (0.292g) were mixed in a three-neck round-bottom flask (three-neck rbf) along with 1.0 ml of DDT, 0.5 ml of oleic acid and 10 ml of ODE. The temperature was controlled using a Digi-Sense standard temperature controller and mixed with a magnetic stirrer set to 1150 rpm. This mixture was degassed under vacuum for 30 minutes at 80℃ and backfilled with argon for 30 minutes. Then, under argon flux, the mixture was taken to 220℃. Samples were collected every 10 minutes during the first hour starting to count immediately after the reacting mixture changed color as the reaction temperature approach 210℃. The second, third and fourth types of QD cores contained zinc and would be referred as core 1-1, core 2-1, and core 4-1 respectively in reference to their zinc to copper initial elemental ratios. The synthesis of these Zn-containing cores followed a similar procedure as that of the Zn-free CIS core. The only difference is that in addition to CuI, $In(Ac)_3$, DDT, oleic acid and ODE,

a zinc precursor, $Zn(St)_2$, was also added to the three-neck rbf containing the mixture (0.16g (0.25mmol), 0.32 g (0.50mmol), and 0.64g (1.0mmol) for 1-1 core, 2-1 core, and 4-1 core respectively). Instead of setting the reaction to 220℃, these reactions were set to 230℃ as the presence of zinc stearate increased the activation energy of the reactions.

Samples were collected every 20 minutes for the first two hours of reaction and every 30 minutes between two and four hours, starting to record time as soon as a change of color in the reaction mixture was observed. Collection was stopped when samples failed to exhibit fluorescent behavior when being exposed to UV-light. Each sample was centrifuged for 15 minutes at 4000 rpm and simultaneously decanted discharging the precipitate. Each sample was optically analyzed as described in the optical analysis section below and the sample exhibiting the highest PL QY was selected to undergo a further cation-exchange reaction.

2.2.2. Synthesis of the core-shell/alloy

For the further coating experiments, a 100 µL sample of QD core mixture was taken from the QD core sample at the reaction time that exhibited the highest PL QY. The core sample was mixed with 1.0 mmol (0.632 g) of zinc stearate, 1.0 mL of DDT, and 10 mL of ODE. The mixture was magnetically stirred under vacuum at 80℃ for 30 minutes and then backfilled with argon for 30 minutes. At this point, the temperature of the mixture was raised to 230℃ and samples were taken after six, 12 and 24 hours of reaction.

2.3. Purification

Five milliliters of QD mixture were extracted three times with a 50/50 hexane-methanol mixture to reduce the amount of unreacted stearate. Then, samples were stored for at least 24

hours in a cool environment to induce precipitation of remaining stearate in solution. The last step of the purification process consisted in precipitating QDs with a 10/1 acetone/hexane solution causing QDs to precipitate out of solution, discharging supernatant.

2.4. Elemental Analysis

To ensure that QDs were dissolved into their component ions, 1.0 mL of concentrated HNO_3 was used to digest QDs solid samples of approximately ten milligrams. Further dilutions were necessary to ensure that the concentration of cations in solutions of each sample to be analyzed fell within range of the standard curve of the instrument utilized to perform this analysis (1ppb -1000 ppb). The water utilized in the dilutions was filtered utilizing a Direct-Q millipore UV filter. For this analysis, an iCAP-6300 inductively coupled plasma mass spectrometer (Thermo Scientific, iCAP Q) was utilized. Copper and zinc elemental traces present in the filtered water were subtracted from final results.

2.5. Optical Analysis

To determine at which times each type of core showed the highest PL QY absorption and emission spectra were taken for each sample collected at various times during the reaction of the QD core, and for each sample collected during the cation-exchange step. Absorption spectra were measured utilizing a Hitachi U-3900H UV/Vis spectrophotometer, and emission spectra were obtained using a Perkin Elmer LS55 Luminescence Spectrometer. The PL QY was calculated by comparison to rhodamine6G, of known QY of 95%. The relation utilized for this calculation is described previously in Equation 4.

Fluorescence lifetimes were obtained of each QD type at zero (QD core), six, 12, and 24 hours of cation exchange using a MicroTime 200 fluorescence microscope (PicoQuant GmbH, Berlin, Germany) modelled from an Olympus IX71 microscope, equipped with a PicoHarp 300 TCSPC controller. A 485 nm laser (PDL 485, Picoquant) excites the QD sample at an operating power of 10 μW. A dichroic mirror (500dcxr, Chroma) is utilized to accomplish a diffraction-limited focus by sending the laser through a water immersion objective (Olympus, Apochromat 60×, NA 1.3). The same objective is used to collect the fluorescent beam passing through the dichroic mirror and a 100 μm diameter pinhole. One long pass fluorescence filter (LP 510, Chroma) is used, and background fluorescence was mitigated by the filter before a single-photon avalanche diode detector (MPD SPAD, Microphotonic Devices, Bolano, Italy).

2.6. Transmission Electron Microscopy (TEM)

Quantum dot cores cand CATEX dissolved in hexane were diluted by a factor of 1000 and 100 respectively and simultaneously cast onto TEM copper grids. The grids were placed in a vacuum oven at 100℃ for 24 hours to allow proper drying.

A size distribution analysis was performed using a JEOL TEM working at a power of 100kV. Images were obtained with an AMT software for TEM imaging and were processed through the software ImageJ to obtain a particle distribution analysis. Images were augmented 400K times their original size resulting in a scale of 4.8 pixels per nanometer, except the Zn-free QD core and CATEX magnified 300K times. In order to obtain a cleaner analysis, it was necessary to subject the images to several process filter features within the ImageJ software to make background uniform and to consolidate poorly resolved particles applying a brightness threshold. After this, the threshold of the image was selected so that only particles with

brightness above this threshold were included in the analysis. The analysis excluded particles that were on the edges and selectively excluded particles that were beyond the size boundaries manually set i.e., clumps or agglomerations of several particles would not be selected by the software as they would display sizes outside a normal distribution for a given sample.

2.7. X-ray Photoelectron Spectroscopy (XPS)

X-ray Photoelectron Spectroscopy Studies were performed utilizing a PHI Versaprobe XPS scanning X-ray monochromator that uses a monochromated Al Kα beam and a dual beam charge neutralization. This apparatus is also equipped with a spherical capacitance analyzer, a multi-channel detector, Ar and C-60 cluster ion guns and angle resolved XPS. The data was analyzed using a Phi Multipak data analysis software.

Chapter 4: Results and Discussion

4.1. Synthesis of the QD core

Once the four reaction mixtures were taken to temperatures close to 200℃ the first changes started to appear as the mixtures became clear and changes in appearance started to occur as showed Figure 5. The mixtures progressively changed from yellow to orange, followed by a red, and lastly a dark red. The Zn-free reaction mixture experienced this change at temperatures near 210℃ like previous reports [8], [23]. Conversely, the Zn-containing reaction mixtures experienced color change at higher temperatures. The core 1-1 and core 2-1 reaction started to change appearance around 226-228℃, and for the core 4-1 the change was not observed until reaching 230℃, implying a higher activation energy that is directly related with increasing the amount of zinc present.

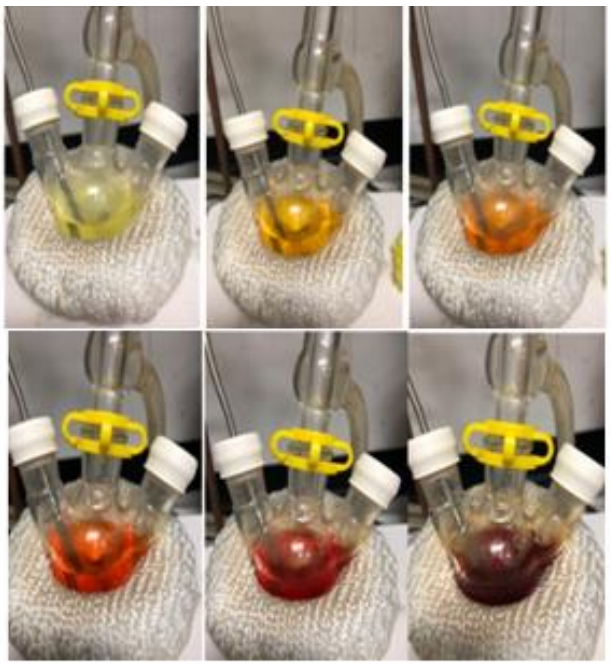

Figure 5 - Beginning of the nucleation reaction during the first minutes of the core synthesis

The Zn-free reaction was the only reacting mixture that was not taken to 230℃, instead 220℃ was deemed appropriate for the nucleation reaction and annealing of atoms to take place while still promoting crystal growth. Samples were taken every ten minutes for the Zn-free QD core reaction and every 20 minutes and 30 minutes for the QD cores 1-1 and 2-1, and every hour for the QD core 4-1.

4.1.1. Emission Spectra

Figure 6 a-d displays the temporal evolution of the emission spectra corresponding to the synthesis reactions of the four QD core reactions studied in this report (Zn-free, 1-1, 2-1 and 4-1 respectively). This figure shows little change on the emission for earlier reaction times but shifts drastically towards the red part of the visible spectrum once a particular time is reached. The time at which the redshift starts to occur seems to be related to the zinc content of the reaction mixture, increasing as the zinc content is incremented. This, again, is evidence that zinc-containing QD core reactions show a higher activation energy.

The Zn-free reaction (Figure 2-a) shows an initial blueshift from ten minutes to 20 minutes, but its longer wavelength emission boundary does not change, which might be caused due to nucleation of smaller particles with remaining monomers in solution after the initial nucleation. Assuming Zn-containing reactions follow a similar growth mechanism as the Zn-free reaction, the early small, nucleated nanocrystals provide base for Ostwald ripening to occur after the larger QDs have reached an optimum crystalline structure.

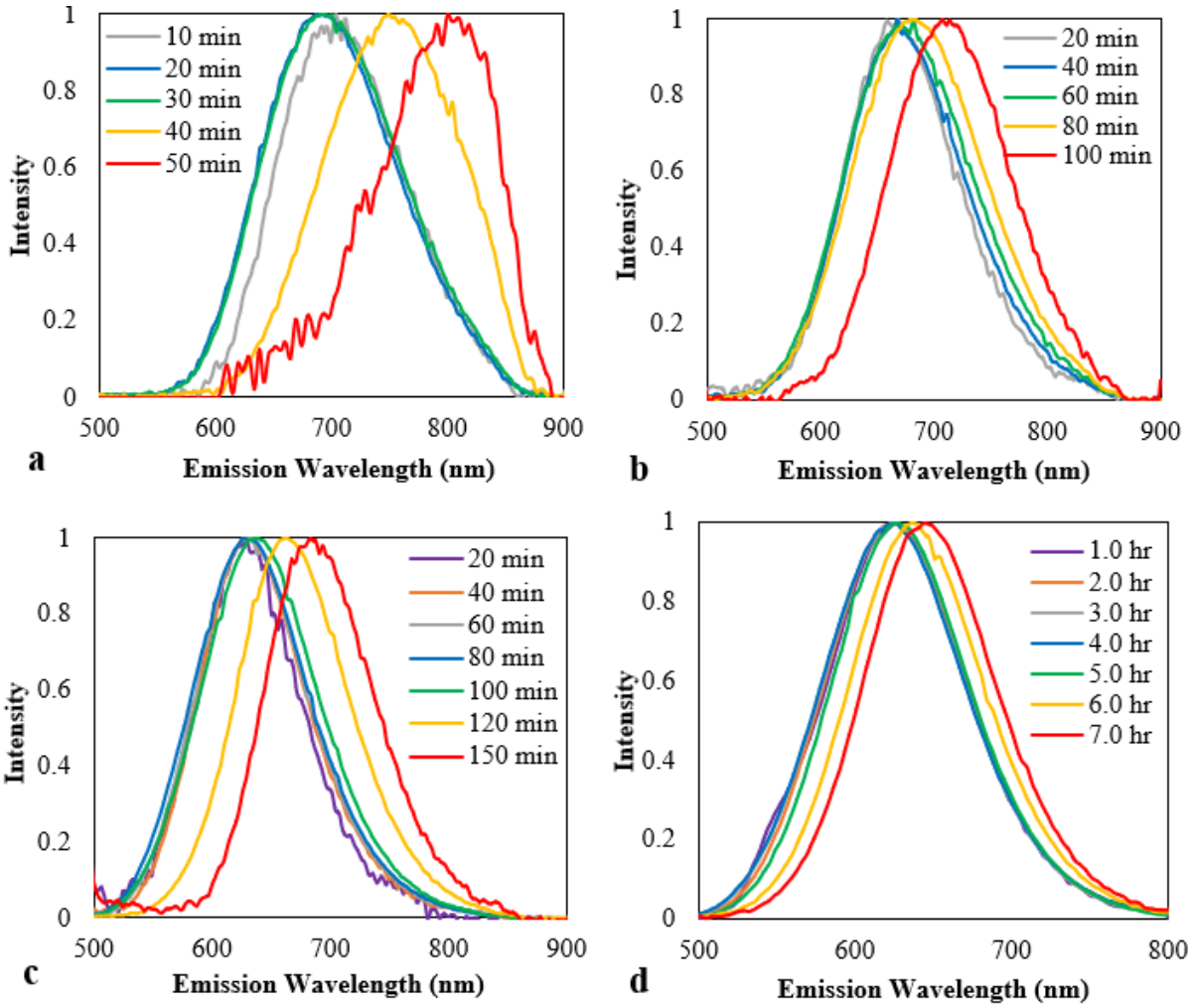

Figure 6 - Temporal evolution of the emission spectra of the QD core synthesis reactions

4.1.2. PL QY of the QD core

The time during the reaction progress at which a prominent redshift starts to occur is specific to each reaction and coincides with the instant at which the maximum PL QY for each reaction is achieved. As a matter of fact, Figure 7-a shows the PL QY characteristics for CIS and CuIn[Zn]S_2 QD cores as their synthesis reaction progresses.

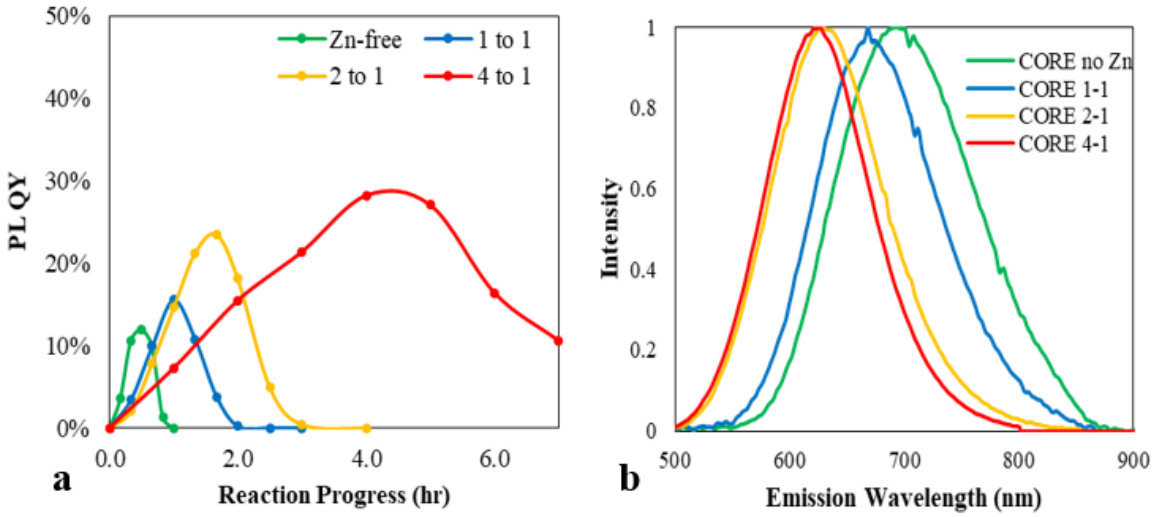

Figure 7 - PL QY and emission spectra of QD cores

Every reaction shows a similar trend in which the PL QY increases until it reaches a maximum optimum PL QY, and subsequently decreases until nanoparticles stop exhibiting fluorescence (except for the 4-1 core that reaches it eventually, but it is not shown due to scalability). This may be because at early stages during the QD core formation the crystallinity of the nanoparticles is impure. However, some lattice defects and traps states are eliminated improving crystallinity until the reaction reaches the best possible PL QY at those conditions of temperature and concentration when an optimum reflux time has lapsed.

4.1.3. Full-width-at-half-maximum (FWHM)

Figure 8 shows an interesting phenomenon observed, the fact that a slower increase in the FWHM is observed during the QD core reactions as the amount of zinc precursor is incremented. Essentially, this suppresses Ostwald ripening, reducing size distribution, hence, obtaining less polydisperse nanocrystals. As a matter of fact, a size-focusing effect at conditions of oversaturation observed in CIS QDs is reported by Talapin et al. [11]. Although Talapin et al. did

not include zinc in the QD core synthesis, zinc-containing reactions in Figure 8 b-d (1-1, 2-1, 4-1 cores respectively) could also follow the same principle under excessive zinc concentrations.

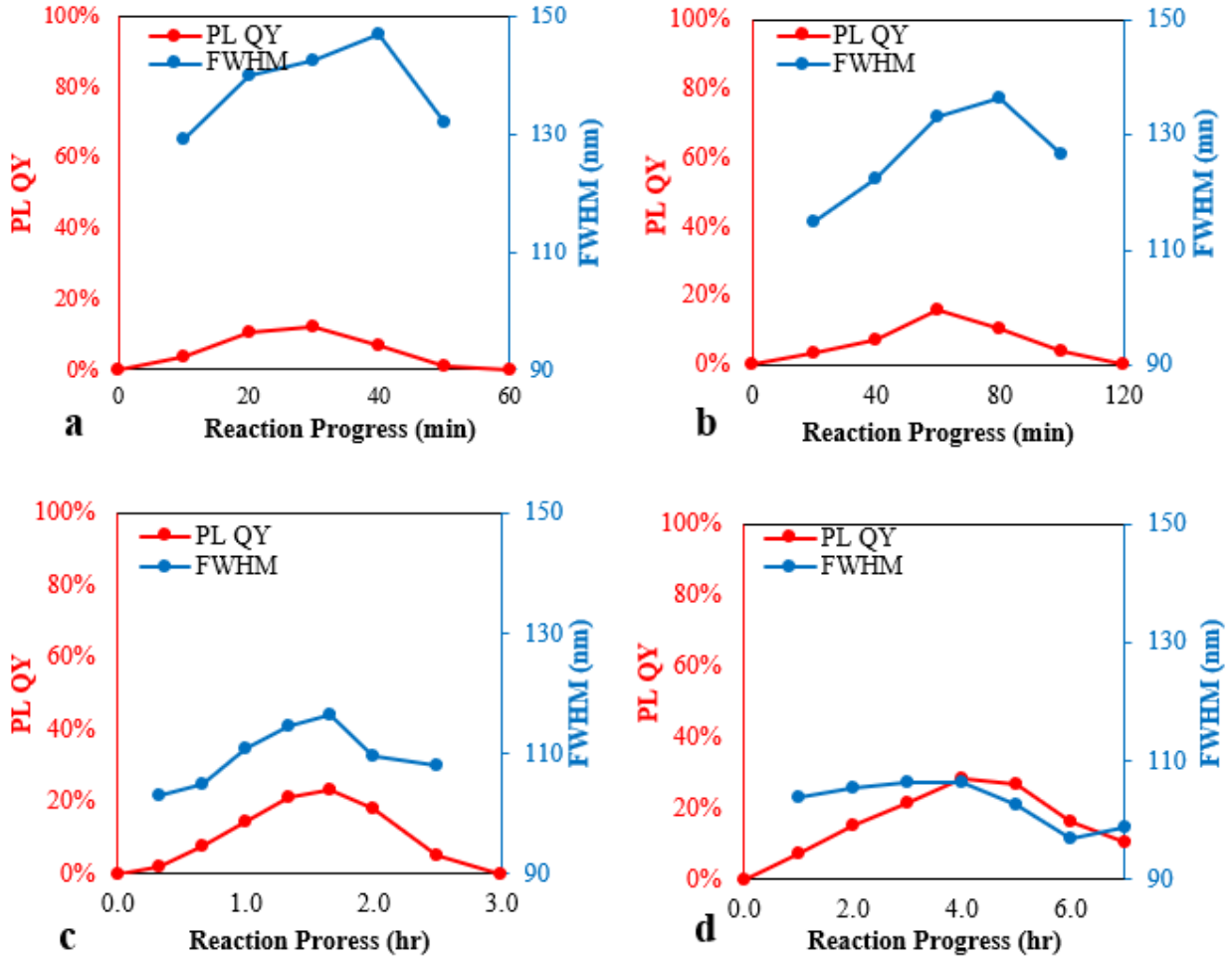

Figure 8 - FWHM and PL QY as QD core synthesis progresses

4.1.4. Maximum Wavelength

Figure 9 shows that the maximum wavelength of the QD cores did not increase during the larger portion of the beginning of the reactions, implying that NCs were able to achieve an optimum size at very early stages of the reactions prior to the collection of the first samples. Although QDs do not seem to increase their size during these early stages, their PL QY is

drastically improved during this lapse of time meaning that QDs continued to improve their crystallinity while maintaining the same size.

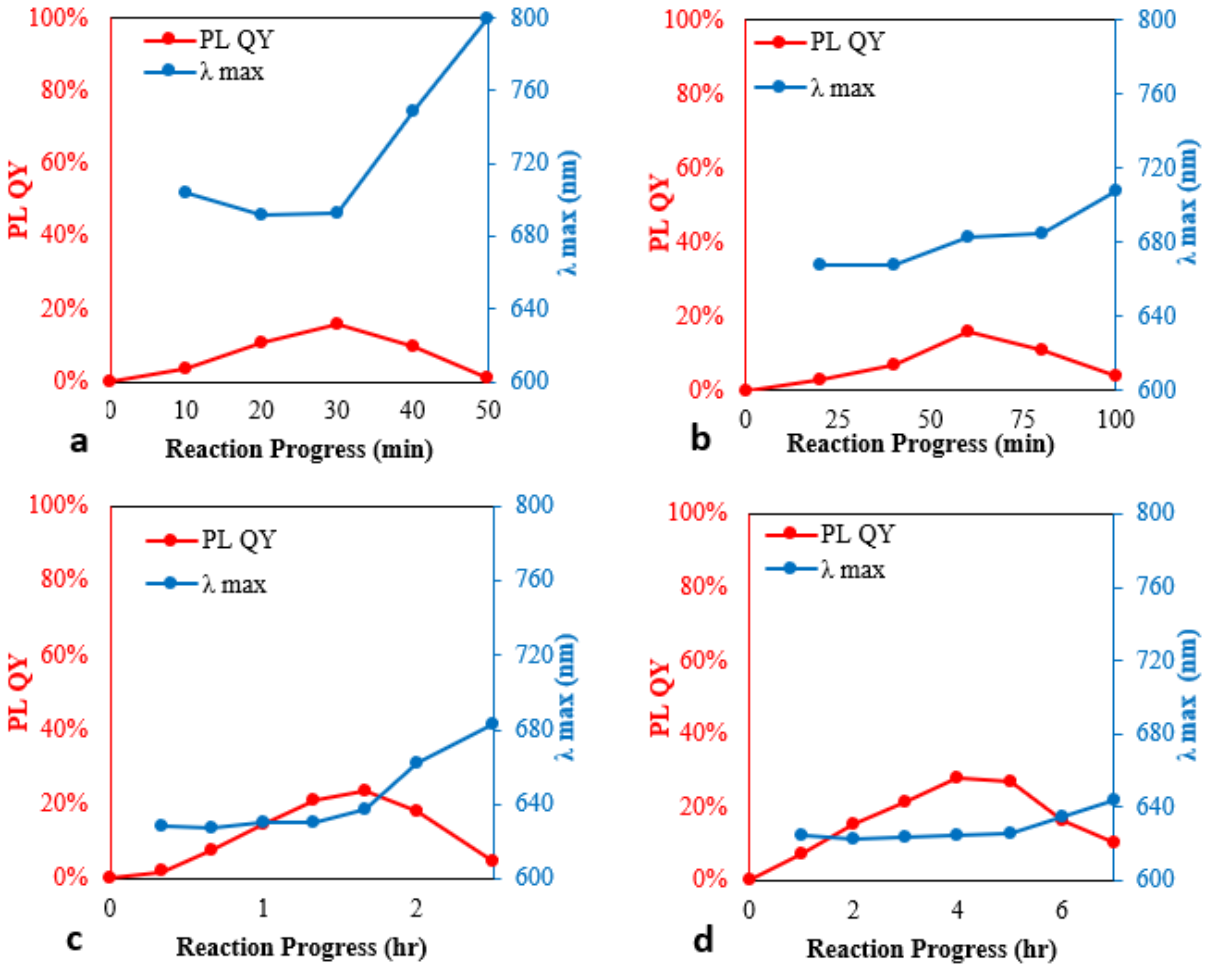

Figure 9 - Maximum emission wavelength and PL QY as core synthesis progresses

The high temperatures at which these reactions proceeded provided enough heat to anneal surface defects and improve crystallinity of optimum-sized QDs, coinciding with reports made by Zhang et al. [51]. Furthermore, looking at the FWHM showed in Figure 8, QDs became more monodisperse during these first stages, which may be caused by Ostwald ripening, one of the governing growth mechanisms in colloidal NCs synthesis [52].

Finally, the dramatic decrease in PL QY could be caused by the prolonged exposure to a high temperature environment resulting in a poor surface passivation as a result of pyrolysis of DDT at high temperatures. This is also supported by Li et al. [46] where they state that at long reflux time, or exceedingly high temperatures, DDT decomposes resulting in the destabilization of NCs due to DDT not only being a sulfur precursor but also a stabilizing ligand. This results in QD precipitation within the reaction, a phenomenon observed in this work and corroborated by looking at data presented by Li et al. [46]

Quantum dot core reactions containing larger amounts of zinc reached higher PL QY while taking longer to achieve this. These reactions also require a higher activation energy than the Zn-free CIS cores. Alloyed QDs have been proven to perform better than non-alloyed QDs, especially when their synthesis is done in one step [53] as opposed to the one-step synthesis of their non-alloyed counterparts. The transition metals copper and zinc tend to produce alloys, which leads one to think that zinc-containing cores are at least partially alloyed.

A slower annealing process appears to be related to a better passivation of QD surface defects, increasing the PL QY, which is achieved over longer prolonged times as zinc composition increases. The presence of zinc equally seems to influence the reduction of Ostwald ripening which then contributes to adding more evidence to the fact that zinc has an important effect on the structural rearrangement of CIS QDs.

4.2. Synthesis of CATEX QDs

Unlike the QD core synthesis where an immediate change was observed when reactions reached 210℃ (for Zn-free) and between 225℃-230℃ (for Zn-containing QD cores), CATEX

reactions did not show an immediate color change. Instead, it happened gradually over the course of six hours.

4.2.1. Emission Spectra

Figure 10 a-d (a-d correspond to the alloying of the Zn-free, 1-1, 201, 4-1 QD cores respectively) shows the temporal evolution of the emission spectra of the second step of QD synthesis, showing an overall blueshift (typical of $CuInS_2$ [8], and other ternary systems). This is contrary to the redshift that typically occurs when shelling binary QD cores such as CdSe.

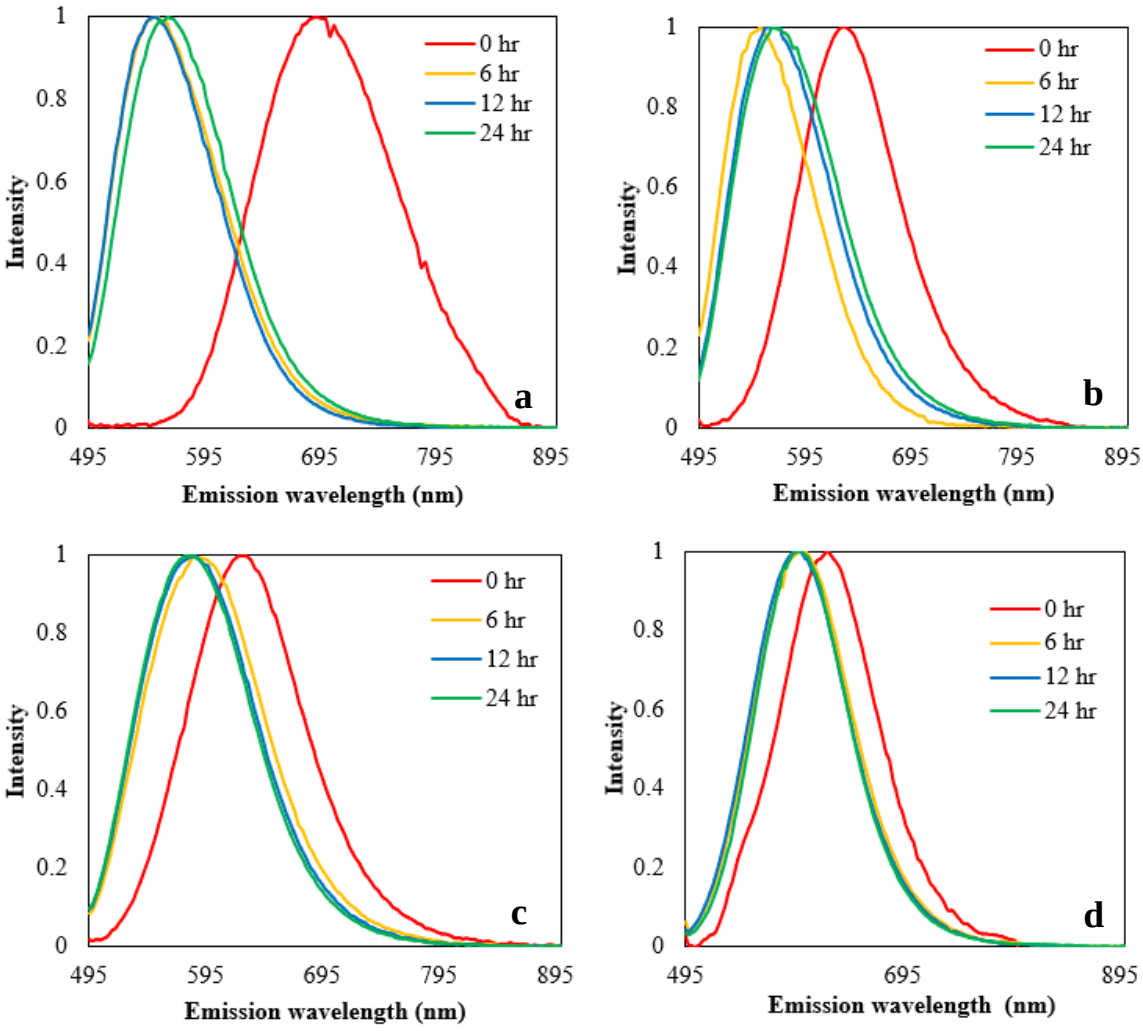

Figure 10 - Emission spectra of CATEX QDs as reaction progresses

4.2.2. PL QY and Maximum Wavelength

The increase in PL QY enhanced by the presence of zinc during the QD core formation is directly related to the inhibition of further PL QY increase during the cation exchange reaction as showed in Figure 11-a. In fact, Figure 11-b shows that the amount of zinc present in QD cores also inhibits the typical blue-shifting tendency of CIS cores upon cation exchange (see emission spectra in Figure 10).

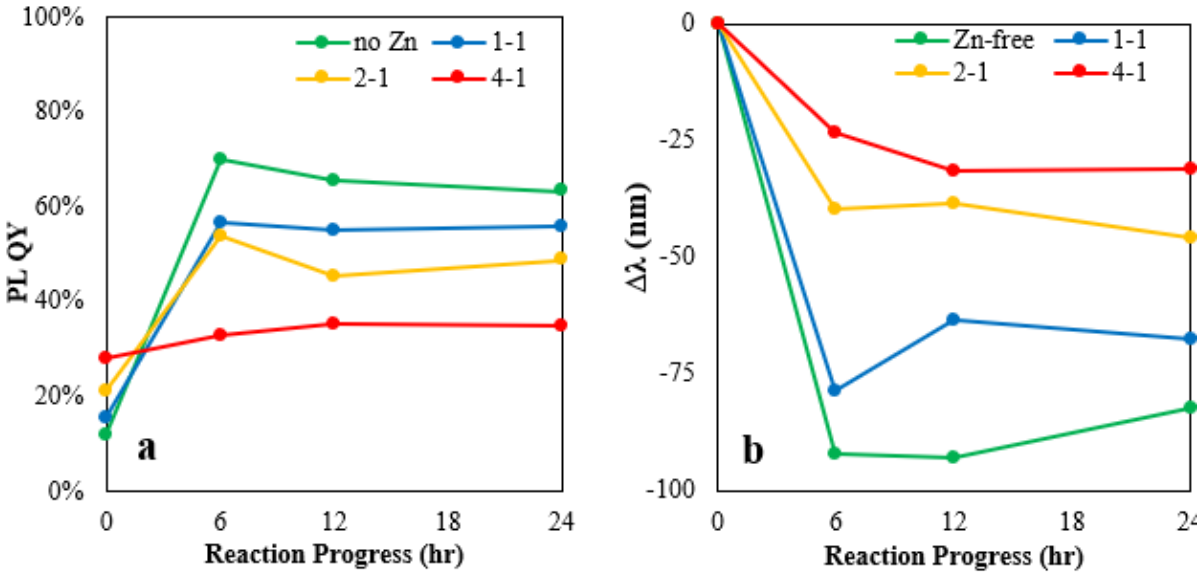

Figure 11- CATEX PL QY and Maximum Wavelength

This implies that the rate at which cation exchange was taking place is lowered by the presence of zinc due to a potential zinc saturation of the NC core. Quantum dots that did not contain Zn initially reported the largest increase in PL QY going from 12% to over 70% upon cation exchange similarly to a previous study performed at Heyes group [23]. Although QD cores that contained zinc improved their PL QY as well (core 1-1 and core 2-1), this gain

occurred at a lower extent to the point that QD cores 4-1 only improved their PL QY by 25% of their QY before coating.

4.2.3. Full-width-at-half-maximum (FWHM)

Figure 12 compares the FWHM with the PL QY for the CATEX reactions, where the Zn-free core CATEX and to a lesser extent, the Zn-free core 1-1 show substantial FWHM shrinking during the first six hours of reaction, contrasted with a great improvement of their PL QY.

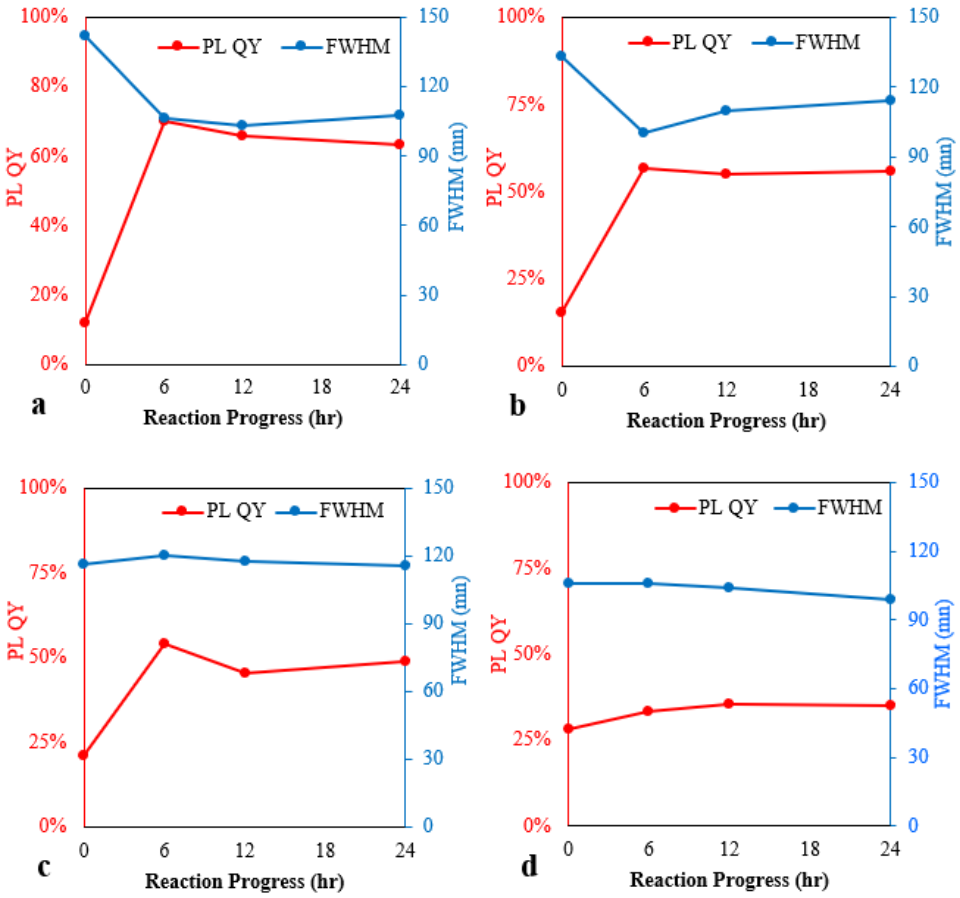

Figure 12 - CATEX PL QY and FWHM

This decrease in FWHM is not showed for the 2-1 and 4-1 core CATEX QDs likely due to QD cores already been saturated with zinc before the start of CATEX reactions.

4.3. Lifetime Measurements

4.3.1. Tau Average

Figure 13 illustrates the increase in fluorescence lifetime exhibited by CATEX nanocrystals during the progress of the cation exchange reactions. The fluorescence lifetime of all four samples converges slightly above 300 ns regardless of their initial lifetime magnitude. Quantum dot cores that contained zinc before the cation exchange reaction took place underwent a lower enhancement of fluorescence lifetime, when compared to Zn-free core CATEX QDs. Again, this is evidence of the fact that saturating the QD core with zinc has a detrimental effect in the enhancement of the radiative properties of CIS NCs.

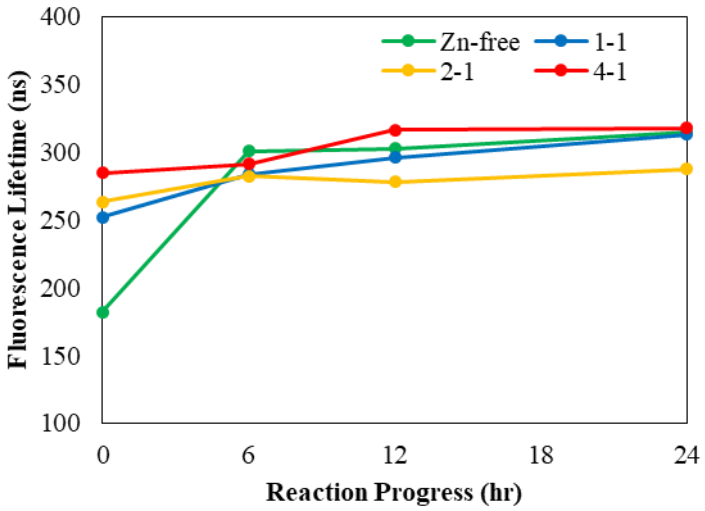

Figure 13 – CATEX QDs tau average measurements

4.3.2. Lifetime Decay

Figure 14 shows the multiexponential lifetime decay functions corresponding to the QD cores before (at zero hours) and after CATEX reactions. The decay functions converge as the

initial amount of zinc is increased, which offer further evidence on smaller rate of cation exchange that takes place in zinc containing QD core samples upon shelling.

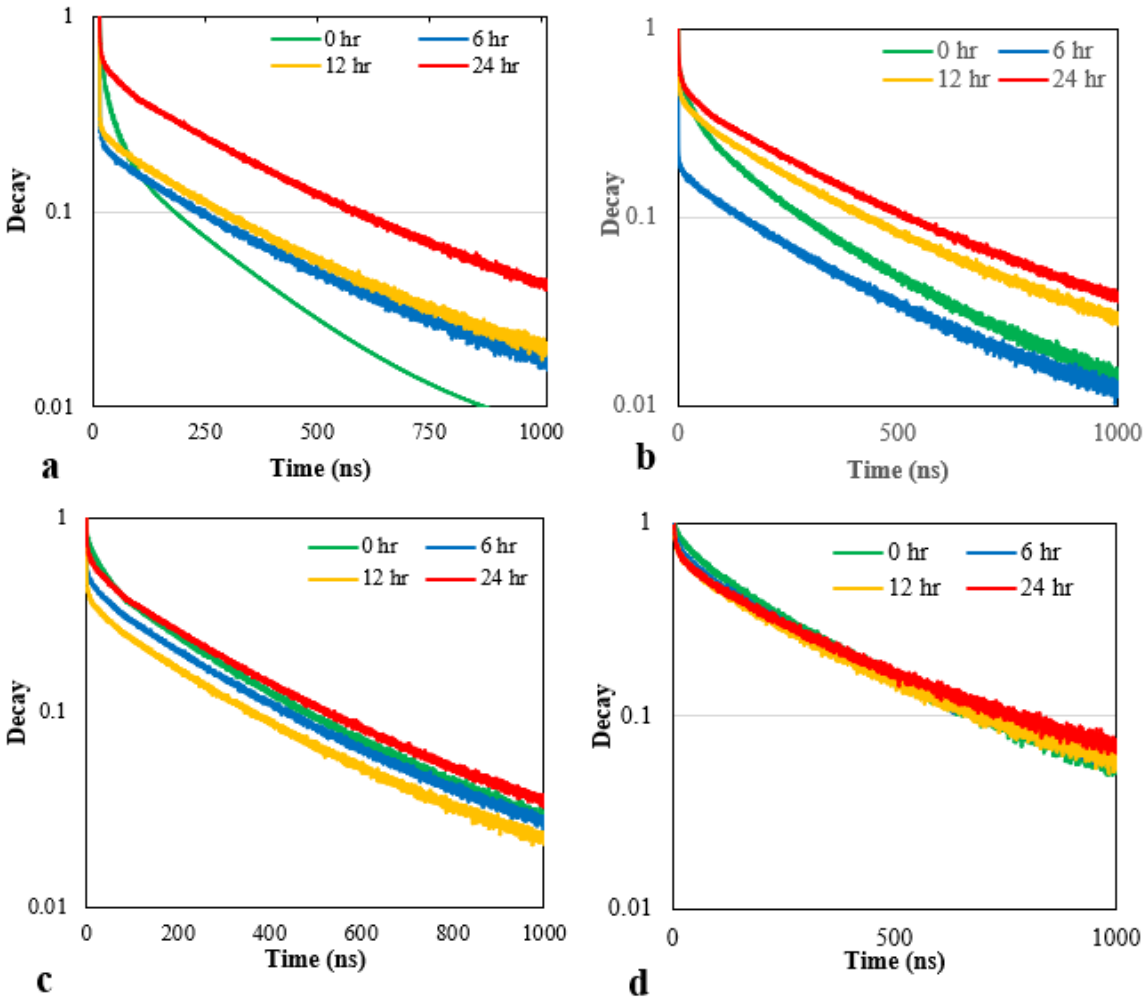

Figure 14 - Lifetime Decay functions for CATEX reactions

4.3.3. Radiative and Non-radiative Rate Constants

Radiative rate constants for all reactions are shown in Figure 15-a, all of which were enhanced upon coating during the CATEX step, expected since both, fluorescence lifetime and PL QY benefitted from coating. Comparatively, non-radiative rate constants decreased implying

a reduction in the number of trap states caused by surface defects and lattice imperfections present in NCs.

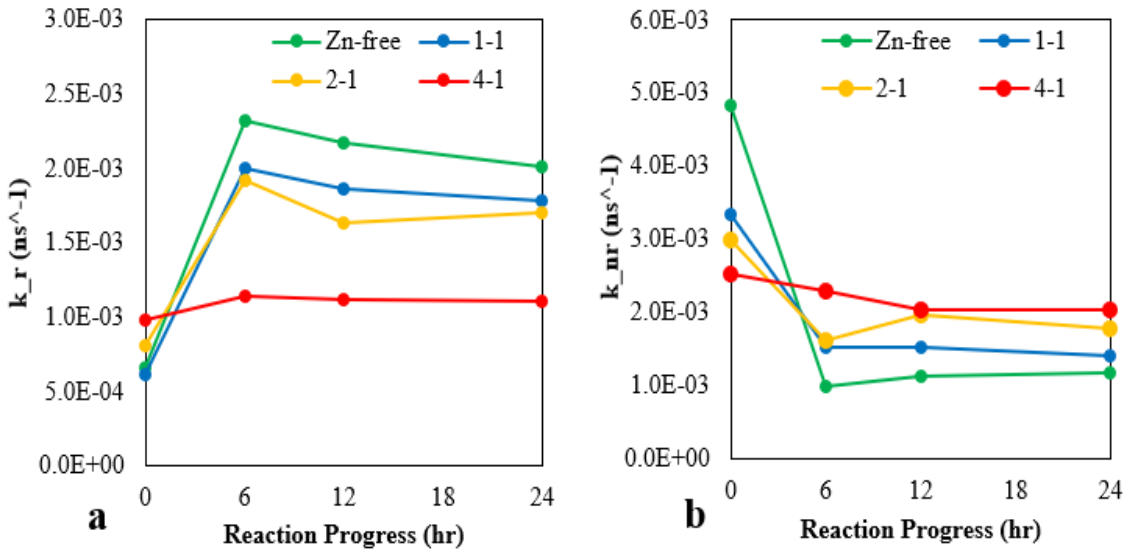

Figure 15 - Radiative and non-radiative rate constants during the CATEX reaction progress

4.5. Elemental Analysis

Elemental analysis measurements displayed in Figure 16 show that an enormous rate of cation exchange and shelling takes place with Zn^{2+} overtaking Cu^{+} and In^{3+} ions, resulting in $CuInS_2$ and $CuIn[Zn]S_2$-doped ZnS QDs, similar to findings reported by Nguyen et al. [23].

Most of the cation replacement of In^{3+} and Cu^{+} ions with Zn^{2+} ions take place within the first six hours of the coating reaction. The right side of Figure16 is plotted in a logarithmic scale, as opposed to a linear plot, to better display indium and copper compositions. Similar to other findings at Heyes' group, $CuInS_2$ and/or $CuIn[Zn]S_2$ small concentrations in the overall QD composition is explained by the present of a predominant ZnS lattice with dopant level amounts of $CuInS_2$ and/or $CuIn[Zn]S_2$ recombination centers[23].

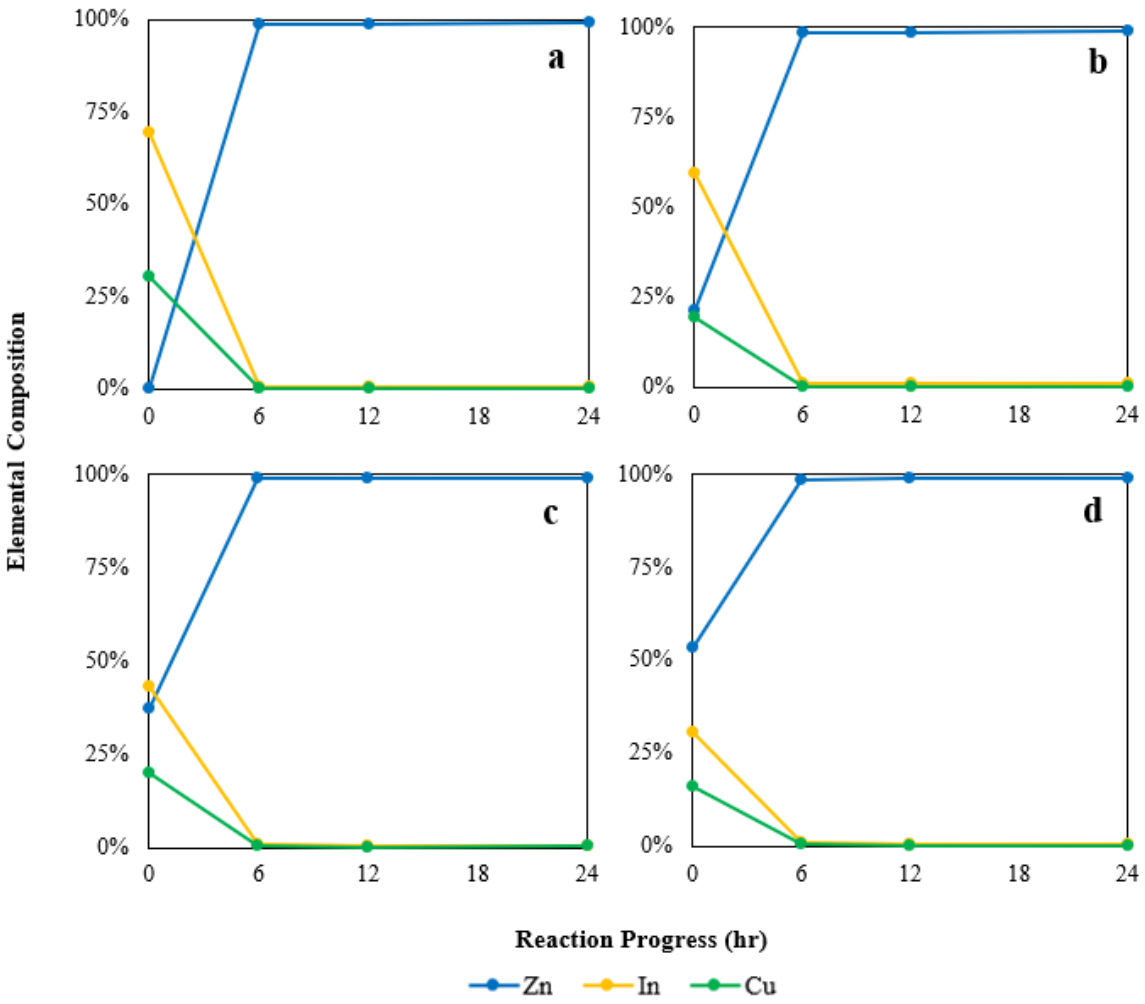

Figure 16 – ICP-MS elemental analysis of the temporal evolution of the CATEX reaction of Zn-free (a), 1-1 (b), 2-1 (c), 4-1(d) QD cores.

4.5.1. Elemental Ratios

Figure 17 contrasts different elemental molar ratios as cation exchange/shelling reactions progress. Taking a closer look at the elemental analysis results it is noticeable a variation in the ratios of the compositions of indium and copper, suggesting that either Cu^{+} or In^{3+} have a preferential exchange with Zn^{2+}.

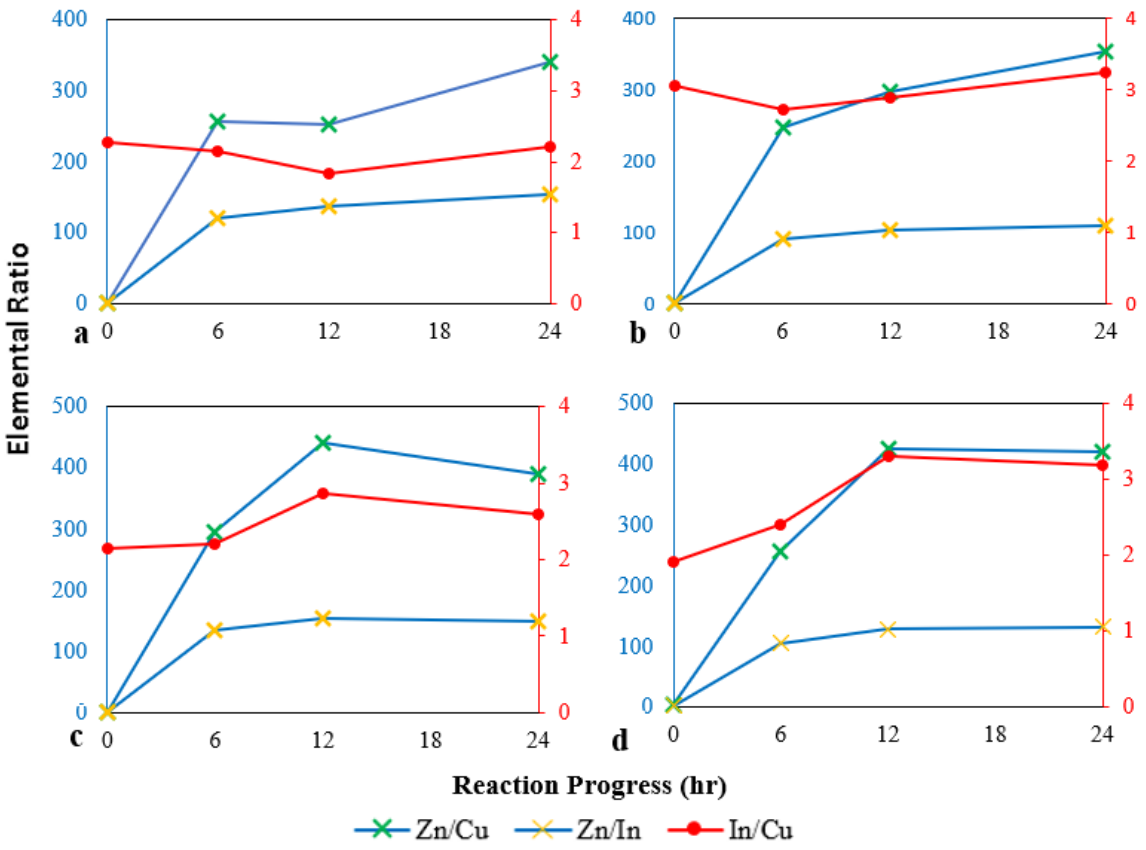

Figure 17- CATEX elemental ratios as reaction progresses

Interestingly enough, while the Zn-to-In ratio reaches a plateau after six hours for all reactions, there still seems to be an ongoing Zn-to-Cu exchange taking place for those reactions that contained the least amount of zinc. This is contrasted with a stagnant Cu-to-In ratio observed in the Zn-free and 1-1 core CATEX reactions. The stagnant In-to-Cu ratio is not observed for the 2-1 and 4-1 Zn-containing core, for which the In-to-Cu ratio increases. A change in In-to-Cu is not stoichiometrically possible unless a simultaneous redox reaction where Cu^{+} is oxidized to Cu^{2+} takes place during the cation exchange of the QD cores. Nevertheless, ICP-MS is unable to provide information on oxidation states of elements present in a sample.

4.6. TEM Imaging

Figure 18 shows TEM images obtained from the Zn-free QD core sample before (left) and after (right) cation exchange/selling reaction taken at a magnification of 300X.

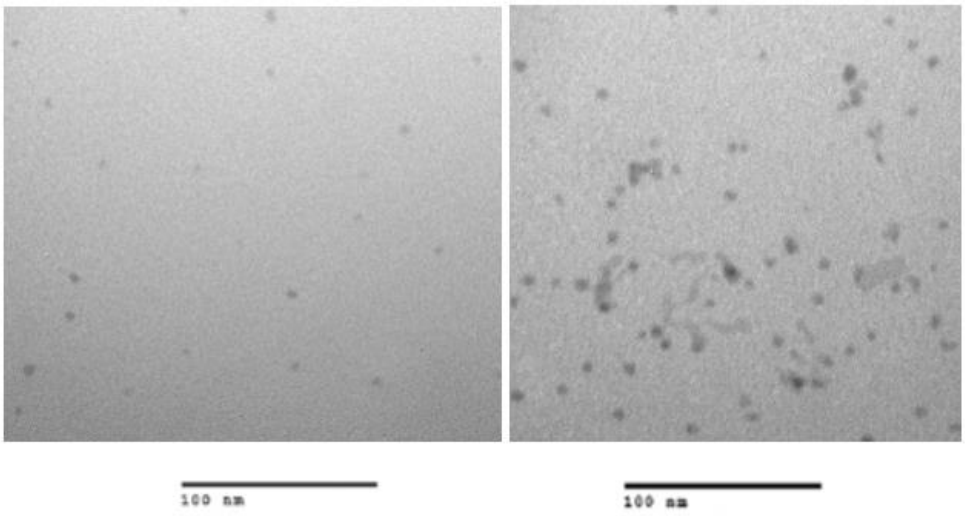

Figure 18 – TEM images of Zn-free QD core before and after CATEX

Figure 19 shows TEM images obtained from Zn-containing QD cores before and after cation exchange reactions. These results are contrasted with the emission spectra in Figure 10, which show that the largest change in wavelength between QD cores and their post-cation exchange counterparts was observed in NCs with lower zinc compositions. Similarly, Figure 19 show that those QD core that achieved larger sizes after cation exchange were those with least zinc. The lack of zinc in CIS QD cores allows a higher rate of In^{3+} and Cu^{+} cations being exchanged by the newly added Zn^{2+} in solution. This process takes place by simultaneously exchanging two Zn^{2+} by one Cu^{+} and one In^{3+} cations.

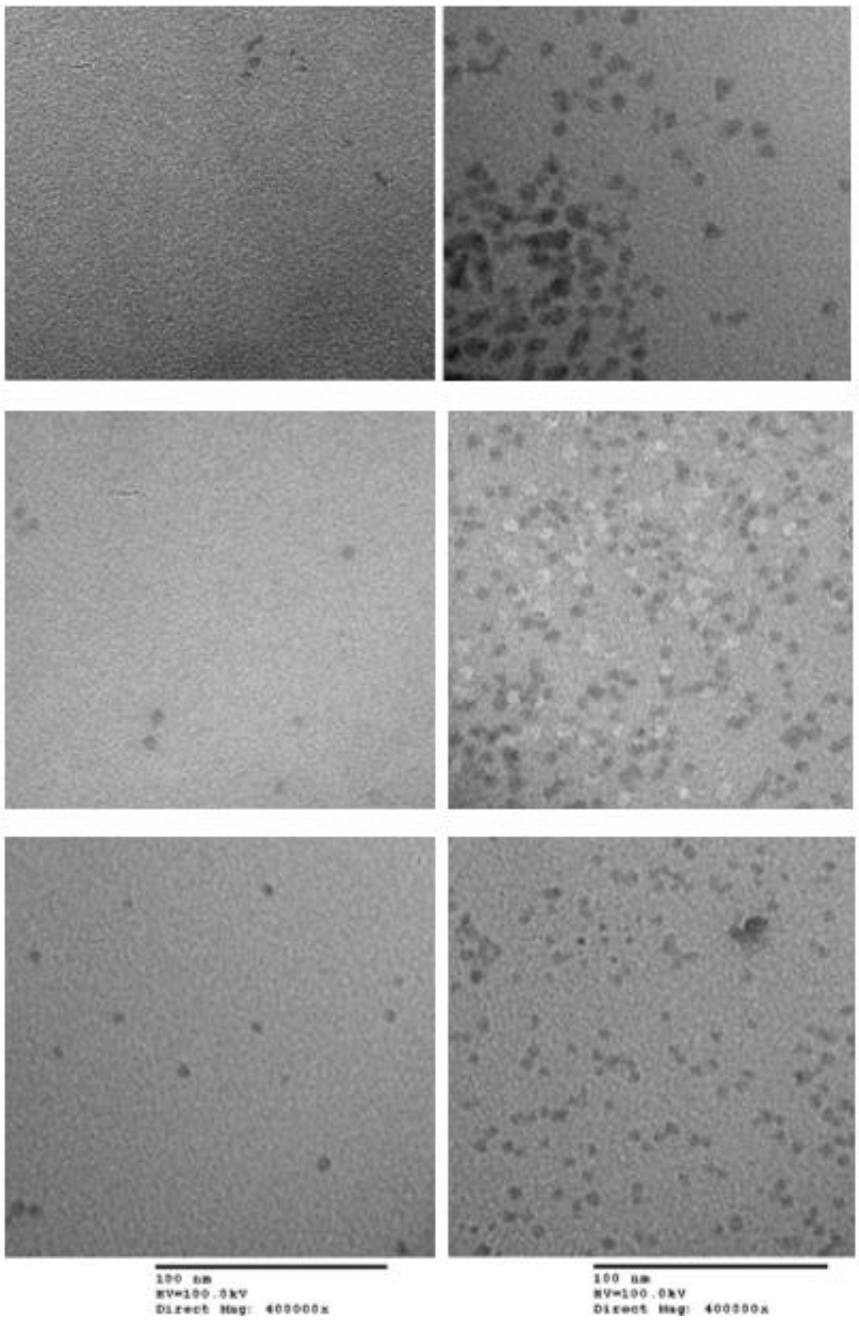

Figure 19 - TEM images of Zn-containing QD cores before and after the cation exchange reactions.

4.6.1. Size Distribution Analysis

A size distribution analysis performed on at least 100 nanoparticles for each sample is displayed in Figure 20.

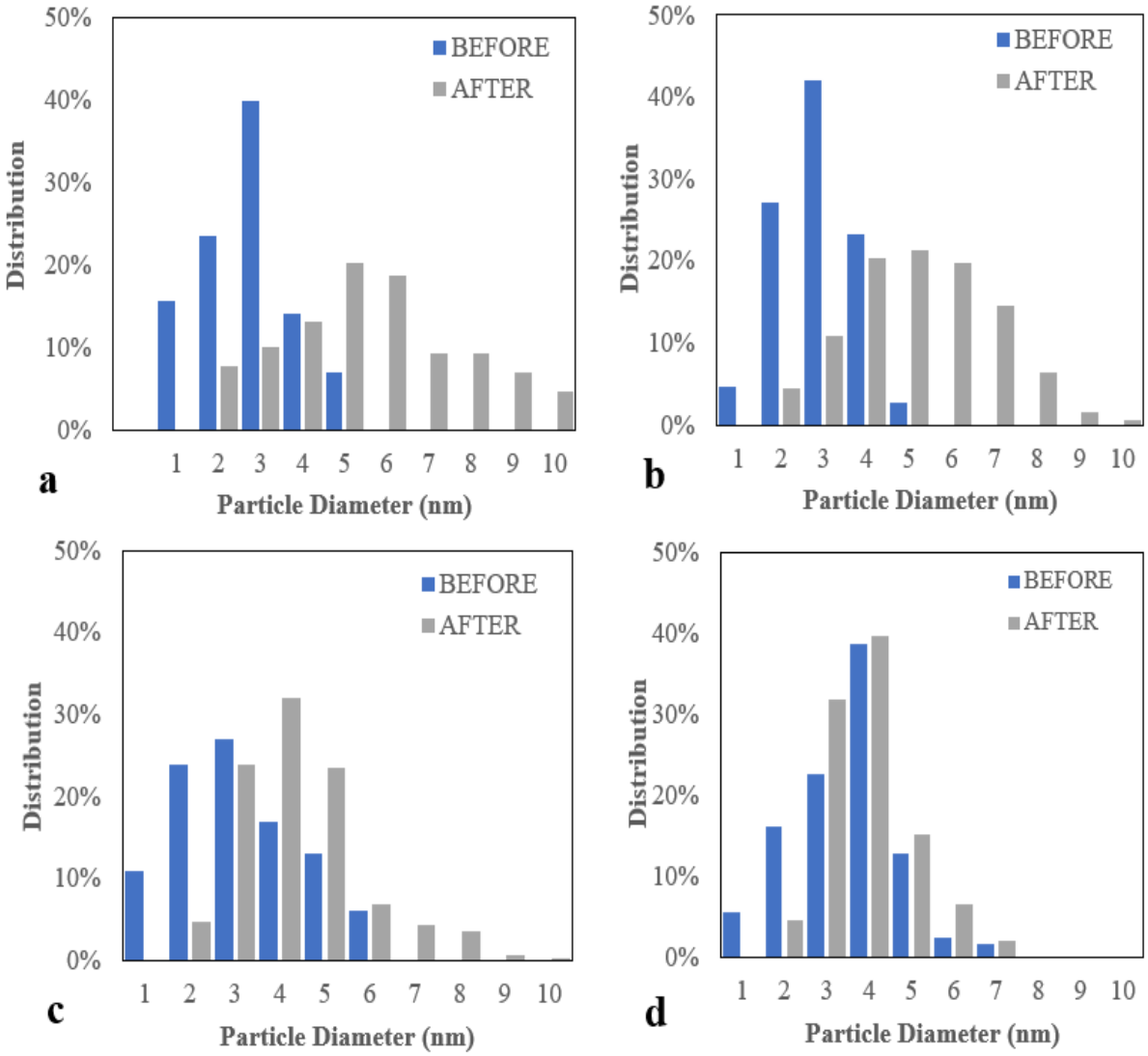

Figure 20 – TEM size distribution analysis of the four cores before and after CATEX

The lack of particle growth for those QD cores that had the most zinc is, again, evidence of zinc-saturated QD cores that are unable to undergo further zinc exchange, and therefore, increase their size. The particle growth and the blue-shifting emission spectra is also evidence of the assumption that after QDs have underwent cation exchange, they possess a partially alloyed architecture as opposed to a pure core/shell.

4.7. XPS Studies

XPS studies performed on QD cores displayed in Figure 21 revealed that it is more likely for In^{3+} ions (Figure 21-a) to be localized on the outer atom layers of QD cores as their XPS signal was significantly higher when compared to those of Cu^{+} (Figure 21-b), and Zn^{2+} (Figure 21-c). This is corroborated by findings reported by Park et al. [8].

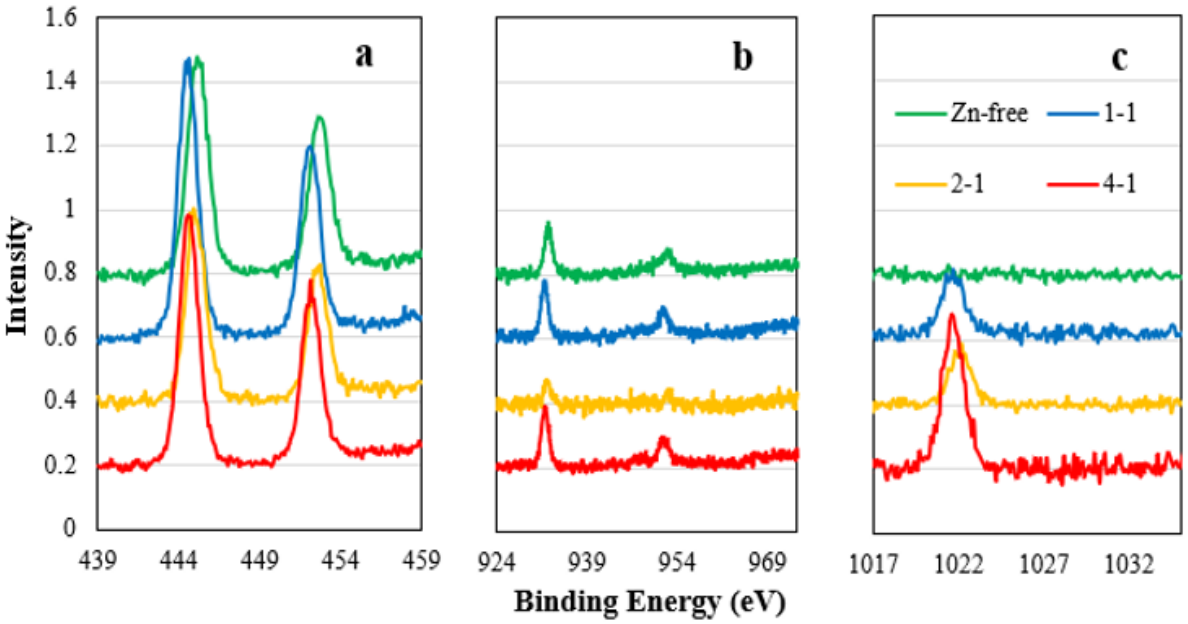

Figure 21 XPS studies reported for QD cores

This is valuable information as it provides further insight on the fact that QD cores are neither a pure homogenous alloy, nor do they exhibit a clear core/shell architecture. Instead, they seem to be partially alloyed nanocrystals that show different ion concentrations along the particle radius. The particles seem to be indium-rich close to the surface, and therefore copper and zinc-rich (only Cu-rich for Zn-free CIS cores) as the canter of the nanoparticle is approached. No evidence of an oxidation of Cu^{+} to Cu^{2+} was found on the QD cores, as the XPS major peak at 932 eV and the satellite peak at 945 correspond both to Cu^{1+}.

A further XPS study was performed on the QDs after they underwent cation exchange for 24 hours but no In^{3+} or Cu^{+} traces were detected in any CATEX sample as can be seen in Figure 22-a and 22-b. Figure 22-c shows the presence of Zn^{2+} ion in all CATEX reactions.

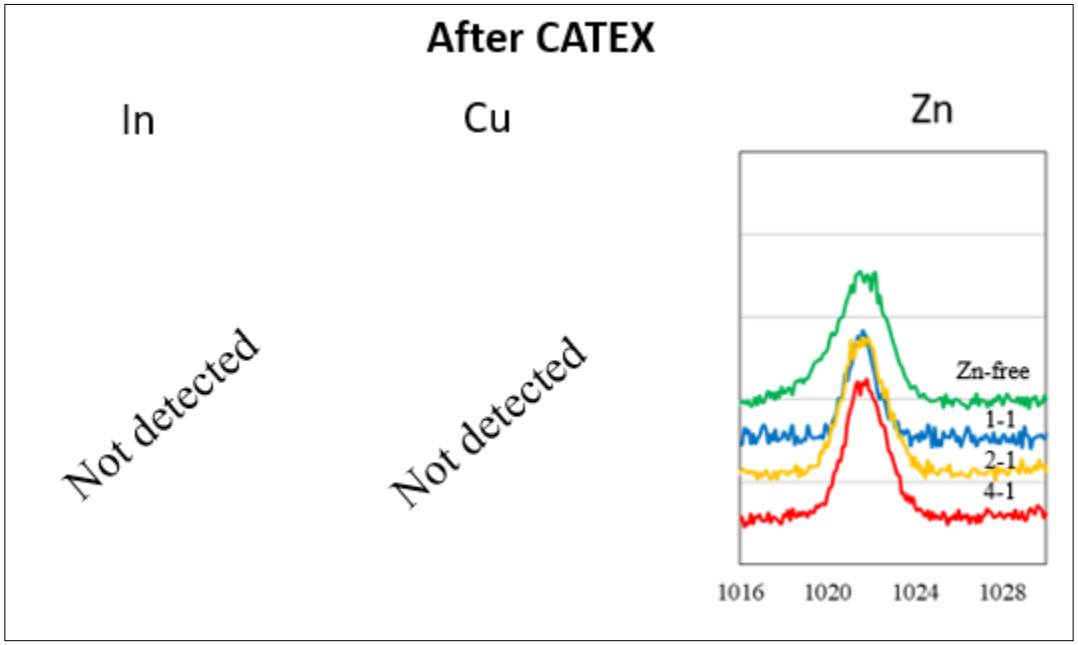

Figure 22 – XPS studies on CATEX QDs after 24 hours of reaction

The lack of Cu^{2+} and In^{3+} peaks on the CATEX QDs XPS analysis after 24 hours of reaction combined with the elemental analysis that confirms the presence of copper and indium in the CATEX QDs could mean one of two things. The detection limit of the XPS analysis failed to reach copper and indium dopant level concentrations (see ICP-MS data in Figure 16), or that both indium and copper are not located anywhere close to the NCs surface.

Undoubtedly, CATEX QDs contain copper and indium as the blueshift observed upon shelling, the emission wavelength showed in the emission spectra (Figure 10) are characteristics of CIS and not ZnS alone.

Chapter 5: Conclusions and Future of Research

5.1 Conclusions

The incorporation of zinc during the synthesis of QD cores of $CuInS_2$/ZnS and $CuIn[Zn]S_2$/ZnS resulted in better optical properties that their Zn-free CIS counterparts, promoting a PL QY increase from 12% to 28%. The fluorescence lifetime was also increased from close to 175 ns for Zn-free QD cores to 300 ns for the 4-1 Zn-containing core. At the QD core level Zn-containing QDs performed better, displaying higher PL QY and better lifetimes optical properties than Zn-free CIS QDs promoting an overall increase of the radiative constant and a decrease on the non-radiative constant. This implies an overall reduction of trap states caused due to surface defects and lattice mismatches.

The presence of zinc in the synthesis of the core has been found to be associated with a reduction of polydispersity of QDs with a decreasing FWHM as more zinc is added to the QD core, implying a size focusing effect at the QD core level. However, Zn-free CIS performed better in terms of their PL QY upon further shelling/cation exchange during the second step of QD synthesis. Although the fluorescence lifetimes of all samples after 24 hours of CATEX was very close, above 300 ns, a sharp difference was observed in their PL QY since upon cation exchange QD cores with higher zinc elemental composition achieved lower PL QY. In contrast the highest PL QY was achieved by Zn-free QD cores, followed by those that had small concentrations of zinc in the core.

The overall elemental composition of the QDs after 24 hours of shelling resulted in NCs that were mostly ZnS (more than 98%) in all instances. The sizes of NCs after 24 hours seemed

to be inversely related to the Zn/(Cu+In) ratios of QD cores. This is further evidence of a lower degree of cation exchange for those QDs with higher zinc concentrations.

XPS studies were unable to confirm the presence of Cu^{2+} in CATEX QDs after 24 hours of reaction, likely due to the dopant level concentrations at which these ions were found in the nanocrystals. XPS studies performed on QD cores revealed that indium peaks were higher than copper peaks implying a preferential localization of indium atoms close to the surface of the nanocrystals. However, upon cation exchange both PL QY and fluorescence lifetime properties were not improved as much as in their zinc-free counterparts.

Zinc-free NCs achieved a PL QY of up to 75%. Although zinc-containing QDs showed better properties during the QD core synthesis, zinc saturation of the core was found to have been on the way of further surface passivation during the cation exchange step. Zn-free QDs reached particle sizes of over 7 nm while a stagnant growth was reported for those QD cores that contained the most Zn. ICP-MS results showed that more than 98% of the composition of QDs after further surface passivation during the CATEX step was mostly zinc with traces of indium, and even less copper. XPS data suggest that the surface of the QD core is indium-rich while the CATEX QDs are composed of a mostly ZnS lattice with dopant level indium and copper compositions.

To summarize, the presence of zinc in the QD core prior further alloying made it impossible for NCs to form a core-shell structure, remaining alloys.

5.2. Future of Research

Due to XPS detection limits not being able to detect ions at dopant level concentrations, it was not possible to detect indium or copper ions in the 24-hour CATEX QDs. Therefore, the

hypothesis of Cu^{2+} and Cu^{+} having a role on the preferential exchange for indium ions could not be confirmed. HR-TEM imaging needs to be performed on these QDs so lattice parameters can be assigned. HR-TEM would also allow us to understand better the degree of alloying and shelling that these QDs present, which in conjecture with XPS data could provide further information on the structural composition and elemental profiling of the QDs.

A meticulous blinking study needs to be performed on these QDs so findings reported on this thesis can be linked to possible mechanisms, and therefore provide better insight on how to control blinking in $CuInS_2$ QDs. A cytotoxicity analysis and a comparison with previous CdSe QDs cytotoxicity analyses should be performed to investigate how benign $CuInS_2$ are when compared to other commercially available QDs.

References

[1] M. A. Kastner, “Artificial Atoms,” *Phys. Today*, vol. 46, no. 1, pp. 24–31, Jan. 1993, doi: 10.1063/1.881393.

[2] M.-S. Hsieh, N.-H. Shiao, and W.-H. Chan, “Cytotoxic Effects of CdSe Quantum Dots on Maturation of Mouse Oocytes, Fertilization, and Fetal Development,” *Int. J. Mol. Sci.*, vol. 10, no. 5, pp. 2122–2135, May 2009, doi: 10.3390/ijms10052122.

[3] S. Nikazar, V. S. Sivasankarapillai, A. Rahdar, S. Gasmi, P. S. Anumol, and M. S. Shanavas, “Revisiting the cytotoxicity of quantum dots: an in-depth overview,” *Biophys. Rev.*, vol. 12, no. 3, pp. 703–718, Jun. 2020, doi: 10.1007/s12551-020-00653-0.

[4] M. J. Gallagher *et al.*, “Release, detection and toxicity of fragments generated during artificial accelerated weathering of CdSe/ZnS and CdSe quantum dot polymer composites,” *Environ. Sci. Nano*, vol. 5, no. 7, pp. 1694–1710, 2018, doi: 10.1039/C8EN00249E.

[5] A. P. Alivisatos, “Semiconductor Clusters, Nanocrystals, and Quantum Dots,” *Science*, vol. 271, no. 5251, pp. 933–937, Feb. 1996, doi: 10.1126/science.271.5251.933.

[6] A. M. Derfus, W. C. W. Chan, and S. N. Bhatia, “Probing the Cytotoxicity of Semiconductor Quantum Dots,” *Nano Lett.*, vol. 4, no. 1, pp. 11–18, Jan. 2004, doi: 10.1021/nl0347334.

[7] Y. Fu, D. Kim, W. Jiang, W. Yin, T. K. Ahn, and H. Chae, “Excellent stability of thicker shell CdSe@ZnS/ZnS quantum dots,” *RSC Adv.*, vol. 7, no. 65, pp. 40866–40872, 2017, doi: 10.1039/C7RA06957J.

[8] J. Park and S.-W. Kim, “CuInS2/ZnS core/shell quantum dots by cation exchange and their blue-shifted photoluminescence,” *J. Mater. Chem.*, vol. 21, no. 11, p. 3745, 2011, doi: 10.1039/c0jm03194a.

[9] J. An *et al.*, “Surface Modification of a Stable CdSeZnS/ZnS Alloy Quantum Dot for Immunoassay,” *J. Nanomater.*, vol. 2020, pp. 1–9, Oct. 2020, doi: 10.1155/2020/4937049.

[10] S. Ghosh *et al.*, “Near-Unity Photoluminescence Quantum Yield and Highly Suppressed Blinking in a Toxic-Metal-Free Quantum Dot,” *J. Phys. Chem. Lett.*, vol. 12, no. 5, pp. 1426–1431, Feb. 2021, doi: 10.1021/acs.jpclett.0c03519.

[11] D. V. Talapin, A. L. Rogach, M. Haase, and H. Weller, “Evolution of an Ensemble of Nanoparticles in a Colloidal Solution: Theoretical Study,” *J. Phys. Chem. B*, vol. 105, no. 49, pp. 12278–12285, Dec. 2001, doi: 10.1021/jp012229m.

[12] T. Yuan, F. Yuan, X. Li, Y. Li, L. Fan, and S. Yang, “Fluorescence–phosphorescence dual emissive carbon nitride quantum dots show 25% white emission efficiency enabling single-

component WLEDs," *Chem. Sci.*, vol. 10, no. 42, pp. 9801–9806, 2019, doi: 10.1039/C9SC03492G.

[13] J. R. Lakowicz, *Principles of Fluorescence Spectroscopy*, 3rd ed. New York: Springer, 2006.

[14] B. R. Fisher, H.-J. Eisler, N. E. Stott, and M. G. Bawendi, "Emission Intensity Dependence and Single-Exponential Behavior In Single Colloidal Quantum Dot Fluorescence Lifetimes," *J. Phys. Chem. B*, vol. 108, no. 1, pp. 143–148, Jan. 2004, doi: 10.1021/jp035756+.

[15] H. Xu, V. Chmyrov, J. Widengren, H. Brismar, and Y. Fu, "Mechanisms of fluorescence decays of colloidal CdSe–CdS/ZnS quantum dots unraveled by time-resolved fluorescence measurement," *Phys. Chem. Chem. Phys.*, vol. 17, no. 41, pp. 27588–27595, 2015, doi: 10.1039/C5CP03109E.

[16] V. Nadtochenko *et al.*, "Multiexponential dynamics of Mn2+(3d5) excitation in manganese doped ZnCdS quantum dots: Stimulated emission band in femtosecond transient spectra reveals ultrafast nonradiative energy transfer to Mn2+(3d5)," *Chem. Phys. Lett.*, vol. 743, p. 137160, Mar. 2020, doi: 10.1016/j.cplett.2020.137160.

[17] A. L. Efros and D. J. Nesbitt, "Origin and control of blinking in quantum dots," *Nat. Nanotechnol.*, vol. 11, no. 8, pp. 661–671, Aug. 2016, doi: 10.1038/nnano.2016.140.

[18] P. Bharadwaj and L. Novotny, "Robustness of Quantum Dot Power-Law Blinking," *Nano Lett.*, vol. 11, no. 5, pp. 2137–2141, May 2011, doi: 10.1021/nl200782v.

[19] N. Amecke, A. Heber, and F. Cichos, "Distortion of power law blinking with binning and thresholding," *J. Chem. Phys.*, vol. 140, no. 11, p. 114306, Mar. 2014, doi: 10.1063/1.4868252.

[20] M. Ye and P. C. Searson, "Blinking in quantum dots: The origin of the grey state and power law statistics," *Phys. Rev. B*, vol. 84, no. 12, p. 125317, Sep. 2011, doi: 10.1103/PhysRevB.84.125317.

[21] F. Gao, P. Bajwa, A. Nguyen, and C. D. Heyes, "Shell-Dependent Photoluminescence Studies Provide Mechanistic Insights into the Off–Grey–On Transitions of Blinking Quantum Dots," *ACS Nano*, vol. 11, no. 3, pp. 2905–2916, Mar. 2017, doi: 10.1021/acsnano.6b08040.

[22] B. Omogo, F. Gao, P. Bajwa, M. Kaneko, and C. D. Heyes, "Reducing Blinking in Small Core–Multishell Quantum Dots by Carefully Balancing Confinement Potential and Induced Lattice Strain: The 'Goldilocks' Effect," *ACS Nano*, vol. 10, no. 4, pp. 4072–4082, Apr. 2016, doi: 10.1021/acsnano.5b06994.

[23] A. T. Nguyen, F. Gao, D. Baucom, and C. D. Heyes, "CuInS $_2$ -Doped ZnS Quantum Dots Obtained via Non-Injection Cation Exchange Show Reduced but Heterogeneous Blinking and Provide Insights into Their Structure–Optical Property Relationships," *J. Phys. Chem. C*, vol. 124, no. 19, pp. 10744–10754, May 2020, doi: 10.1021/acs.jpcc.0c01933.

[24] B. Dong *et al.*, "Facile Synthesis of Highly Photoluminescent Ag $_2$ Se Quantum Dots as a New Fluorescent Probe in the Second Near-Infrared Window for in Vivo Imaging," *Chem. Mater.*, vol. 25, no. 12, pp. 2503–2509, Jun. 2013, doi: 10.1021/cm400812v.

[25] J. Liu, X. Zhao, H. Xu, Z. Wang, and Z. Dai, "Amino Acid-Capped Water-Soluble Near-Infrared Region CuInS $_2$ /ZnS Quantum Dots for Selective Cadmium Ion Determination and Multicolor Cell Imaging," *Anal. Chem.*, vol. 91, no. 14, pp. 8987–8993, Jul. 2019, doi: 10.1021/acs.analchem.9b01183.

[26] M. F. Foda, L. Huang, F. Shao, and H.-Y. Han, "Biocompatible and Highly Luminescent Near-Infrared CuInS $_2$ /ZnS Quantum Dots Embedded Silica Beads for Cancer Cell Imaging," *ACS Appl. Mater. Interfaces*, vol. 6, no. 3, pp. 2011–2017, Feb. 2014, doi: 10.1021/am4050772.

[27] Y. Nakamura, Y. Iso, and T. Isobe, "Bandgap-Tuned CuInS $_2$ /ZnS Core/Shell Quantum Dots for a Luminescent Downshifting Layer in a Crystalline Silicon Solar Module," *ACS Appl. Nano Mater.*, vol. 3, no. 4, pp. 3417–3426, Apr. 2020, doi: 10.1021/acsanm.0c00175.

[28] S. M. Kobosko and P. V. Kamat, "Indium-Rich AgInS $_2$ –ZnS Quantum Dots—Ag-/Zn-Dependent Photophysics and Photovoltaics," *J. Phys. Chem. C*, vol. 122, no. 26, pp. 14336–14344, Jul. 2018, doi: 10.1021/acs.jpcc.8b03001.

[29] J.-Y. Chang, J.-M. Lin, L.-F. Su, and C.-F. Chang, "Improved Performance of CuInS $_2$ Quantum Dot-Sensitized Solar Cells Based on a Multilayered Architecture," *ACS Appl. Mater. Interfaces*, vol. 5, no. 17, pp. 8740–8752, Sep. 2013, doi: 10.1021/am402547e.

[30] M. Frasco and N. Chaniotakis, "Semiconductor Quantum Dots in Chemical Sensors and Biosensors," *Sensors*, vol. 9, no. 9, pp. 7266–7286, Sep. 2009, doi: 10.3390/s90907266.

[31] M. Chern, J. C. Kays, S. Bhuckory, and A. M. Dennis, "Sensing with photoluminescent semiconductor quantum dots," *Methods Appl. Fluoresc.*, vol. 7, no. 1, p. 012005, Jan. 2019, doi: 10.1088/2050-6120/aaf6f8.

[32] M. Peng *et al.*, "Room-Temperature Direct Synthesis of PbSe Quantum Dot Inks for High-Detectivity Near-Infrared Photodetectors," *ACS Appl. Mater. Interfaces*, p. acsami.1c13723, Oct. 2021, doi: 10.1021/acsami.1c13723.

[33] G.-S. Li, D.-Q. Zhang, and J. C. Yu, "A New Visible-Light Photocatalyst: CdS Quantum Dots Embedded Mesoporous TiO $_2$," *Environ. Sci. Technol.*, vol. 43, no. 18, pp. 7079–7085, Sep. 2009, doi: 10.1021/es9011993.

[34] Y. Yuan, N. Jin, P. Saghy, L. Dube, H. Zhu, and O. Chen, “Quantum Dot Photocatalysts for Organic Transformations,” *J. Phys. Chem. Lett.*, vol. 12, no. 30, pp. 7180–7193, Aug. 2021, doi: 10.1021/acs.jpclett.1c01717.

[35] W. Cao, Y. Qin, H. Huang, B. Mao, Y. Liu, and Z. Kang, “Extraction of High-Quality Quantum Dot Photocatalysts via Combination of Size Selection and Electrochemiluminescence,” *ACS Sustain. Chem. Eng.*, vol. 7, no. 24, pp. 20043–20050, Dec. 2019, doi: 10.1021/acssuschemeng.9b05787.

[36] T. Wang, X. Guan, H. Zhang, and W. Ji, “Exploring Electronic and Excitonic Processes toward Efficient Deep-Red CuInS $_2$ /ZnS Quantum-Dot Light-Emitting Diodes,” *ACS Appl. Mater. Interfaces*, vol. 11, no. 40, pp. 36925–36930, Oct. 2019, doi: 10.1021/acsami.9b13108.

[37] Z. Liu *et al.*, “Micro-light-emitting diodes with quantum dots in display technology,” *Light Sci. Appl.*, vol. 9, no. 1, p. 83, Dec. 2020, doi: 10.1038/s41377-020-0268-1.

[38] G. Ba, Q. Xu, X. Li, Q. Lin, H. Shen, and Z. Du, “Quantum dot light-emitting diodes with high efficiency at high brightness via shell engineering,” *Opt. Express*, vol. 29, no. 8, p. 12169, Apr. 2021, doi: 10.1364/OE.421029.

[39] U. Resch-Genger, M. Grabolle, S. Cavaliere-Jaricot, R. Nitschke, and T. Nann, “Quantum dots versus organic dyes as fluorescent labels,” *Nat. Methods*, vol. 5, no. 9, pp. 763–775, Sep. 2008, doi: 10.1038/nmeth.1248.

[40] P. Linkov, V. Krivenkov, I. Nabiev, and P. Samokhvalov, “High Quantum Yield CdSe/ZnS/CdS/ZnS Multishell Quantum Dots for Biosensing and Optoelectronic Applications,” *Mater. Today Proc.*, vol. 3, no. 2, pp. 104–108, 2016, doi: 10.1016/j.matpr.2016.01.033.

[41] Y. Pan *et al.*, “Size controlled synthesis of monodisperse PbTe quantum dots: using oleylamine as the capping ligand,” *J. Mater. Chem.*, vol. 22, no. 44, p. 23593, 2012, doi: 10.1039/c2jm15540k.

[42] S. Liu *et al.*, “Efficiently Passivated PbSe Quantum Dot Solids for Infrared Photovoltaics,” *ACS Nano*, vol. 15, no. 2, pp. 3376–3386, Feb. 2021, doi: 10.1021/acsnano.0c10373.

[43] J.-H. Jo *et al.*, “InP-Based Quantum Dots Having an InP Core, Composition-Gradient ZnSeS Inner Shell, and ZnS Outer Shell with Sharp, Bright Emissivity, and Blue Absorptivity for Display Devices,” *ACS Appl. Nano Mater.*, vol. 3, no. 2, pp. 1972–1980, Feb. 2020, doi: 10.1021/acsanm.0c00008.

[44] Q. Fan, A. Dehankar, T. K. Porter, and J. O. Winter, “Effect of Micelle Encapsulation on Toxicity of CdSe/ZnS and Mn-Doped ZnSe Quantum Dots,” *Coatings*, vol. 11, no. 8, p. 895, Jul. 2021, doi: 10.3390/coatings11080895.

[45] J. C. Kays, A. M. Saeboe, R. Toufanian, D. E. Kurant, and A. M. Dennis, “Shell-Free Copper Indium Sulfide Quantum Dots Induce Toxicity *in Vitro* and *in Vivo*,” *Nano Lett.*, vol. 20, no. 3, pp. 1980–1991, Mar. 2020, doi: 10.1021/acs.nanolett.9b05259.

[46] L. Li, T. J. Daou, I. Texier, T. T. Kim Chi, N. Q. Liem, and P. Reiss, “Highly Luminescent $CuInS_2$/ZnS Core/Shell Nanocrystals: Cadmium-Free Quantum Dots for In Vivo Imaging,” *Chem. Mater.*, vol. 21, no. 12, pp. 2422–2429, Jun. 2009, doi: 10.1021/cm900103b.

[47] C. Würth, M. G. González, R. Niessner, U. Panne, C. Haisch, and U. R. Genger, “Determination of the absolute fluorescence quantum yield of rhodamine 6G with optical and photoacoustic methods – Providing the basis for fluorescence quantum yield standards,” *Talanta*, vol. 90, pp. 30–37, Feb. 2012, doi: 10.1016/j.talanta.2011.12.051.

[48] K. Tillmann and W. J ger, “Quantitative HRTEM analysis of semiconductor quantum dots,” *J. Electron Microsc. (Tokyo)*, vol. 49, no. 2, pp. 245–257, Jan. 2000, doi: 10.1093/oxfordjournals.jmicro.a023804.

[49] S. Wilschefski and M. Baxter, “Inductively Coupled Plasma Mass Spectrometry: Introduction to Analytical Aspects,” *Clin. Biochem. Rev.*, vol. 40, no. 3, pp. 115–133, Aug. 2019, doi: 10.33176/AACB-19-00024.

[50] D. R. Baer, “Guide to making XPS measurements on nanoparticles,” *J. Vac. Sci. Technol. A*, vol. 38, no. 3, p. 031201, May 2020, doi: 10.1116/1.5141419.

[51] J. Zhang, W. Sun, L. Yin, X. Miao, and D. Zhang, “One-pot synthesis of hydrophilic $CuInS_2$ and $CuInS_2$–ZnS colloidal quantum dots,” *J Mater Chem C*, vol. 2, no. 24, pp. 4812–4817, 2014, doi: 10.1039/C3TC32564D.

[52] M. Kahlweit, “Ostwald ripening of precipitates,” *Adv. Colloid Interface Sci.*, vol. 5, no. 1, pp. 1–35, Aug. 1975, doi: 10.1016/0001-8686(75)85001-9.

[53] H. Osman *et al.*, “One-step hot injection synthesis of gradient alloy CdxZn1-xSySe1-y quantum dots with large-span self-regulating ability,” *J. Lumin.*, vol. 206, pp. 565–570, Feb. 2019, doi: 10.1016/j.jlumin.2018.10.089.

Appendix A: Description of Research for Popular Publication

Since the early 2000s heavy metal free Quantum Dots (QDs) have attempted to replace the use of heavy metal containing QDs. $CuInS_2$/ZnS QDs are a potentially less toxic alternative to CdSe. Their two-step synthesis process involves the fabrication of $CuInS_2$ nanocrystals (NCs) followed by the incorporation of zinc precursors. Instead of the traditional core/shell architecture that binary QDs exhibit, $CuInS_2$ coating takes place via ion-exchange resulting in cation exchanged alloyed or partially alloyed QDs (CATEX QDs). The effect that zinc has on the optical properties of $CuInS_2$ NCs was studied by incorporating zinc during the first step of the synthesis.

The incorporation of zinc in the Qs core resulted in QD cores with photoluminescence quantum yields twice and thrice of those CIS core QDs. However, upon cation exchange Zn-free QYs performed better achieving QYs of more than 70%, while the presence of zinc in the core after cation exchange seemed to have a detrimental effect on the optical properties of the NCs, not achieving PL QYs as high as those of the Zn-free NCs. Th addition of zinc prior cation exchange did not seem to have a significant effect on the fluorescence lifetime observed, and their copper and indium composition was still found to be in the dopant level. Monodispersity on the other hand was improved, as well as the particle size kept below five nanometers.

Appendix B: Executive Summary of Newly Created Intellectual Property

It has been found that adding a ZnS shell to $CuInS_2$ cores causes a blue-shift in the emission spectrum, rather than the red-shift that is observed in Cd-based QDs. This is due to a certain degree of ion exchange between copper and/or indium and zinc occurring in the Core. The effects of incorporating Zn into the core prior to shelling on the electronic and optical properties of $CuInS_2$-ZnS cation-exchanged QDs were not studied prior this investigation. This study involved the characterization of the structure and composition of these nanocrystals using XPS, TEM and ICP-MS methods. The results obtained in this study were compared to fluorescence quantum yield, fluorescence lifetime data to make correlations between the composition/architecture of the nanocrystals and the optical properties to determine the possible mechanisms underlying the optical properties.

Appendix C: Potential Patent and Commercialization Aspects of Listed Intellectual Property Items

C.1 Patentability of Intellectual Property (Could Each Item be Patented)

The incorporation of zinc in the QD core of $CuInS_2$ prior its shelling/cation exchange was investigated in this thesis. Due to the fact that this modification of $CuInS_2$ resulted in optical and electronic properties that were similar, if not inferior to those already widely studied in previous publications, these items will not be considered for future patentability.

C.2 Commercialization Prospects (Should Each Item Be Patented)

$CuInS_2$ have a great potential to be used in several fields within the semiconductors industry. However, this investigation targeted applications such as bioimaging, bio-tracking and as fluorescent probes in fluorescence lifetime imaging microscopy (FLIM). However, this investigation was merely done from an academic perspective.

C.3 Possible Prior Disclosure of IP

Disclosure of intellectual property is not necessary at this time since this study was performed from a merely academic perspective.

Appendix D: Broader Impact of Research

D.1 Applicability of Research Methods to Other Problems

This investigation is primarily concerned with the utility of $CuInS_2$-ZnS QDs in applications within the field of single-molecule spectroscopy. Furthermore, the fact that $CuInS_2$-ZnS QDs have lifetimes 10-50-fold longer than some of their binary counterparts opens doors in applications based on fluorescence lifetime such as fluorescence-lifetime imaging microscopy (FLIM).

D.2 Impact of Research Results on U.S. and Global Society

$CuInS_2$-ZnS QDs are heavy-metal-free alternatives to their traditional cadmium-based counterparts which are the most commercialized QDs in the market. QDs have a wide range of applications in fields such as biology, LEDs, photovoltaic devices, and photodetectors.

D.3 Impact of Research Results on the Environment

The fact that $CuInS_2$-ZnS QDs are heavy metal free makes them excellent candidates to replace traditional QDs, especially in biological applications. This could effectively mean to partial of full replacement of heavy metal containing CdSe QDs, which are the most widely used QDs in the market.

Appendix E: Microsoft Project for MS MicroEP Degree Plan

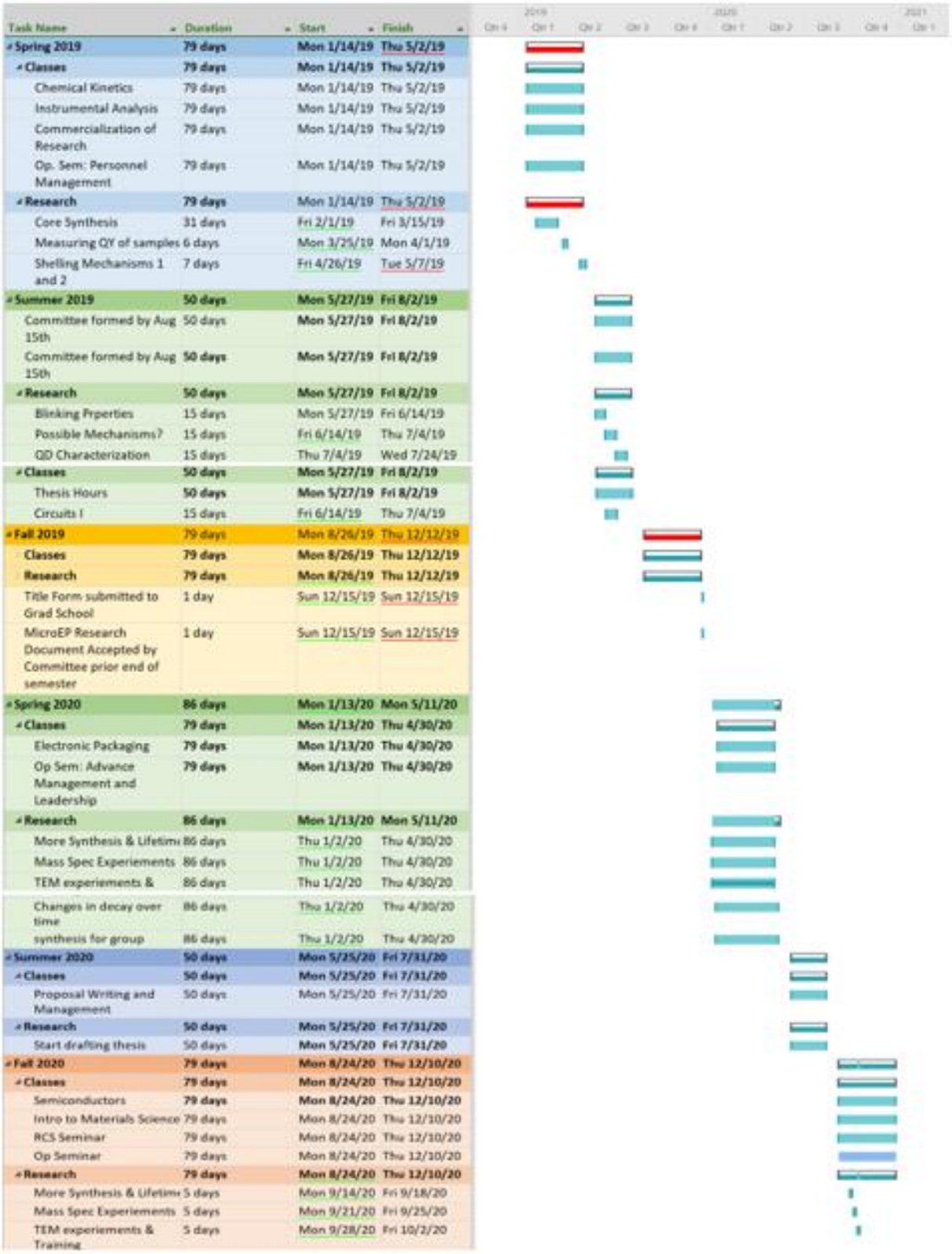

Task Name	Duration	Start	Finish
Spring 2019	**79 days**	**Mon 1/14/19**	**Thu 5/2/19**
Classes	**79 days**	**Mon 1/14/19**	**Thu 5/2/19**
Chemical Kinetics	79 days	Mon 1/14/19	Thu 5/2/19
Instrumental Analysis	79 days	Mon 1/14/19	Thu 5/2/19
Commercialization of Research	79 days	Mon 1/14/19	Thu 5/2/19
Op. Sem: Personnel Management	79 days	Mon 1/14/19	Thu 5/2/19
Research	**79 days**	Mon 1/14/19	Thu 5/2/19
Core Synthesis	31 days	Fri 2/1/19	Fri 3/15/19
Measuring QY of samples	6 days	Mon 3/25/19	Mon 4/1/19
Shelling Mechanisms 1 and 2	7 days	Fri 4/26/19	Tue 5/7/19
Summer 2019	**50 days**	**Mon 5/27/19**	**Fri 8/2/19**
Committee formed by Aug 15th	50 days	**Mon 5/27/19**	**Fri 8/2/19**
Committee formed by Aug 15th	**50 days**	**Mon 5/27/19**	**Fri 8/2/19**
Research	**50 days**	**Mon 5/27/19**	**Fri 8/2/19**
Blinking Prperties	15 days	Mon 5/27/19	Fri 6/14/19
Possible Mechanisms?	15 days	Fri 6/14/19	Thu 7/4/19
QD Characterization	15 days	Thu 7/4/19	Wed 7/24/19
Classes	**50 days**	**Mon 5/27/19**	**Fri 8/2/19**
Thesis Hours	**50 days**	**Mon 5/27/19**	**Fri 8/2/19**
Circuits I	15 days	Fri 6/14/19	Thu 7/4/19
Fall 2019	79 days	Mon 8/26/19	Thu 12/12/19
Classes	**79 days**	**Mon 8/26/19**	**Thu 12/12/19**
Research	**79 days**	**Mon 8/26/19**	**Thu 12/12/19**
Title Form submitted to Grad School	1 day	Sun 12/15/19	Sun 12/15/19
MicroEP Research Document Accepted by Committee prior end of semester	1 day	Sun 12/15/19	Sun 12/15/19
Spring 2020	**86 days**	**Mon 1/13/20**	**Mon 5/11/20**
Classes	**79 days**	**Mon 1/13/20**	**Thu 4/30/20**
Electronic Packaging	**79 days**	**Mon 1/13/20**	**Thu 4/30/20**
Op Sem: Advance Management and Leadership	**79 days**	**Mon 1/13/20**	**Thu 4/30/20**
Research	**86 days**	**Mon 1/13/20**	**Mon 5/11/20**
More Synthesis & Lifetim	86 days	Thu 1/2/20	Thu 4/30/20
Mass Spec Experiements	86 days	Thu 1/2/20	Thu 4/30/20
TEM experiements &	86 days	Thu 1/2/20	Thu 4/30/20
Changes in decay over time	86 days	Thu 1/2/20	Thu 4/30/20
synthesis for group	86 days	Thu 1/2/20	Thu 4/30/20
Summer 2020	**50 days**	**Mon 5/25/20**	**Fri 7/31/20**
Classes	**50 days**	**Mon 5/25/20**	**Fri 7/31/20**
Proposal Writing and Management	50 days	Mon 5/25/20	Fri 7/31/20
Research	**50 days**	**Mon 5/25/20**	**Fri 7/31/20**
Start drafting thesis	50 days	**Mon 5/25/20**	**Fri 7/31/20**
Fall 2020	**79 days**	**Mon 8/24/20**	**Thu 12/10/20**
Classes	**79 days**	**Mon 8/24/20**	**Thu 12/10/20**
Semiconductors	**79 days**	**Mon 8/24/20**	**Thu 12/10/20**
Intro to Materials Science	79 days	Mon 8/24/20	Thu 12/10/20
RCS Seminar	79 days	Mon 8/24/20	Thu 12/10/20
Op Seminar	79 days	Mon 8/24/20	Thu 12/10/20
Research	**79 days**	**Mon 8/24/20**	**Thu 12/10/20**
More Synthesis & Lifetim	5 days	Mon 9/14/20	Fri 9/18/20
Mass Spec Experiements	5 days	Mon 9/21/20	Fri 9/25/20
TEM experiements & Training	5 days	Mon 9/28/20	Fri 10/2/20

Spring 2021	**85 days**	**Mon 1/11/21**	**Fri 5/7/21**
Research	**85 days**	**Mon 1/11/21**	**Fri 5/7/21**
XPS Experiments	7 days	Mon 1/11/21	Tue 1/19/21
TEM Characterization	7 days	Tue 1/19/21	Wed 1/27/21
Refining Lifetime data	21 days	Mon 2/1/21	Mon 3/1/21
Classes	**85 days**	**Mon 1/11/21**	**Fri 5/7/21**
Thesis Hours	**85 days**	**Mon 1/11/21**	**Fri 5/7/21**
Single Molecule Spectroscopy	85 days	Mon 1/11/21	Fri 5/7/21
Summer 2021	**70 days**	**Mon 5/24/21**	**Fri 8/27/21**
Classes	**70 days**	**Mon 5/24/21**	**Fri 8/27/21**
Thesis Hours	70 days	Mon 5/24/21	Fri 8/27/21
Research	**70 days**	Mon 5/24/21	Fri 8/27/21
TEM (CORE)	25 days	Mon 5/24/21	Fri 6/25/21
Fall 2021	**85 days**	**Mon 8/23/21**	**Fri 12/17/21**
Classes	**84 days**	**Mon 8/23/21**	**Thu 12/16/21**
Quantum Chemistry	**84 days**	**Mon 8/23/21**	**Thu 12/16/21**
Research	**79 days**	**Mon 8/23/21**	**Thu 12/9/21**
XPS (CATEX)	5 days	**Mon 8/23/21**	**Fri 8/27/21**
XPS (CORE)	5 days	**Wed 9/1/21**	**Tue 9/7/21**
TEM (CATEX)	7 days	Fri 9/10/21	Mon 9/20/21
Graduation Tasks	**56 days**	**Fri 10/1/21**	**Fri 12/17/21**
Submit Final Copy of Thesis	1 day	Sat 4/10/21	Sat 4/10/21
Apply for Graduation	1 day	Fri 10/1/21	Fri 10/1/21
First Draft Ready	1 day	Fri 11/5/21	Fri 11/5/21
Public Presentation	1 day	Mon 11/22/21	Mon 11/22/21
Defend Thesis	1 day	Wed 12/1/21	Wed 12/1/21
Commencement	1 day	Fri 12/17/21	Fri 12/17/21

Appendix F: Identification of All Software Used in Research and Thesis Generation

Computer #1:

Model Number: INTEL® CORE™ QUAD CPU Q6600

Serial Number: 00392-918-5000002-85671

Location: CHBC 119

Owner: Dr. Colin Heyes

Computer #2:

Model Number: Dell Precision T3400

Serial Number: 76487-OEM-0011903-00102

Location: CHBC 119

Owner: Dr. Colin Heyes

Software #1:

Name: Windows VISTA® HOME BASIC OEMAct

Purchased by: Colin Heyes

Software #2:

Name: Windows® Pro OA

Purchased by: Colin Heyes

Appendix G: All Publications Published, Submitted and Planned

This study has not resulted in the publishing of any academic papers, nor has one been submitted so far. However, when blinking data is collected on these QDs Heyes' Research Group plans on submitting a paper for review and potential publication.